1 **Archaeometrical results related to Neolithic amphibolite stone implements from**

2 **Northeast Hungary**

3 **Erika Kereskényi[a], György Szakmány[b], Béla Fehér[a], Ildikó Harsányi[c], Veronika Szilágyi[c],**

4 **Zsolt Kasztovszky[c], Tivadar M. Tóth[d]**

5 *[a]Department of Mineralogy of Herman Ottó Museum, Kossuth u. 13, H-3525 Miskolc, Hungary*

6 *[b]Department of Petrology and Geochemistry, Eötvös Loránd University, Pázmány Péter sétány*

7 *1/c, H-1117 Budapest, Hungary*

8 *[c]Nuclear Analysis and Radiography Department, Centre for Energy Research, PO Box 49, H-*

9 *1525 Budapest 114, Hungary*

10 *[d]Department of Mineralogy, Geochemistry and Petrology, University of Szeged, Egyetem u. 2,*

11 *H-6722 Szeged, Hungary*

12

13

14 Abstract: 28 amphibolite Neolithic polished stone implements deriving from different archaeological localities and cultures

15 in Northeast Hungary (Borsod-Abaúj-Zemplén County) were archaeometrically analysed by mainly non-destructive methods

16 (MS, EDS/SEM, PGAA). Bulk chemistry of the samples showing subalkali characteristics. The amphibolite polished stone tools

17 were divided into two groups based on their mineral components and metamorphic evolution. A single Ca-amphibole

18 approach was used to calculate peak P-T conditions to determine a thermobarometric model for the amphibolite implements.

19 Data of the studied samples were compared to those of the nearest amphibolite outcrops in Gemericum, Veporicum,

20 Tatricum and Zemplinikum (Slovakia). The Variscan P-T loop covered the thermobarometric data of the analysed stone

21 implements and the amphibolite outcrops. The source areas are assumed to be these fields and/or the crossing riverbeds

22 flowing through them to Borsod-Abaúj-Zemplén County, the archaeological collecting territory of the amphibolite stone axes.

23

24 **Keywords:** amphibolite, polished stone tools, provenance field, Neolithic, Hungary

25

26 Mineral abbreviations: A*mp*: amphibole; M*g-hb*: magnesio-hornblende; *Mg-f-hb*: magnesio-ferri-hornblende; F*hb*:

27 Ferro-hornblende; *Act*: actinolite; F*act*: ferro-actinolite; S*dg:* sadanagaite; F*sdg*: ferro-sadanagaite; *Tsch*: tschermakite; F*e2-*

28 *ftsch*: Ferro-ferri-tschermakite; *ftsch*: Ferro-tschermakite; *f3-ts*: Ferri-Tschermakite; P*rg*: pargasite; F*prg*: ferro-pargasite; a*ug*:

29 Augite; D*i*: diopside; C*px:* clinopyroxene; A*b*: albite; O*lg*: oligoclase; *And*: andesine; L*ab*: labradorite; B*yt*: bytownite; Pl:

30 plagioclase; K*fs:* K-feldspar; E*p*: epidote; C*zo*: clinozoisite; *Chl*: chlorite; B*i*: biotite; *Ms*: muscovite; P*h*: phengite; *Qtz*: quartz;

31 T*tn*: titanite; *Ilm*: ilmenite; M*gt*: magnetite; A*p*: hydroxylapatite; P*y*: pyrite; C*al*: calcite. Jrs: jarosite.

32

33 **1. Introduction**

34   In this paper we present the results of an archaeometrical research program on the polished

35 stone implement collection of the Herman Ottó Museum in Hungary which started in 2014. The

36 collecting area covers Borsod-Abaúj-Zemplén County in Northeast Hungary. The museum owns

37 approximately 500 Neolithic polished stone implements, most of which are metabasites or more

38 specifically in some cases blueschists (Kereskényi et al., 2018), but a significant number of volcanic and

39 sedimentary stone implements are possessed as well according to our observations. Until now 28 tools

40 have been shown to be made of amphibolite. Stone tools which are reached and characterized by the

41 amphibolite facies assemblage; hornblende and plagioclase feldspar, were classified as amphibolite.

42 Contact metamorphosed metabasites are not included among these lithotypes.

43   The archaeological localities where these amphibolite polished stone tools were found are

44 shown in Fig. 1. Most of the findings have an archaeological context, but 10 of the axes were stray finds

45 (Table 1). Borsod/Derékegyháza (Edelény) and Szerencs/Taktaföldvár are the sites with the two largest

46 sets of finds. The Borsod/Derékegyháza (Edelény) locality belongs to the Middle Neolithic Bükk culture

47 (Kalicz & Makkay, 1977). The Szerencs/Taktaföldvár locality represents the late Neolithic Tisza culture

48 (Selján, 2005). Tiszadorogma (Kalicz and Makkay, 1977) and Tiszavalk/Kenderföldek are related to the

49 Alföld Linear Pottery culture (Csengeri, 2013). Findings from Szirmabesenyő and its vicinity (Kalicz and

50 Makkay, 1977) and Miskolc/Aldi2 are linked to the Bükk or Alföld Linear Pottery cultures (Csengeri,

51 2011). The Hejőkürt/Lidl locality is related to the early Tiszadob culture (Csengeri, 2015). The Emőd

52 locality belongs to one or more of the Alföld Linear Pottery, Tiszadob, Tiszadob-Bükk or Bükk cultures

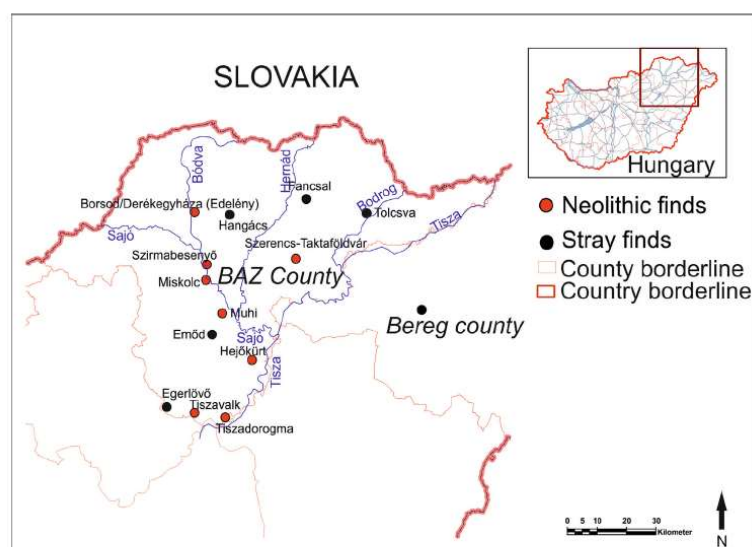53 according to the related ceramics (Csengeri, 2013) (Table 1).

Fig. 1. Schematic map showing archaeological localities of amphibolite stone tools that are deposited at the Herman Ottó Museum. Abbreviation: *BAZ*: Borsod-Abaúj-Zemplén.

54

55

Table 1
Amphibolite implements from the collection of the Herman Ottó Museum giving the different analytical methods and magnetic susceptibility (MS) values in units of 10^{-3} Sl. (Y: yes; N: no; *: "Original surface", semi-quantitative method; AVK: Alföld Linear Pottery).

Sample	Inventory number	Locality	EDS/SEM	PGAA	MS	Archaeological typology	Age	Culture/Phase
B04	70.1.23	Szerencs-Taktaföldvár	Y	Y	0.73	Flat chisel	Late Neolithic	Tisza
B05	70.1.24	Szerencs-Taktaföldvár	Y	Y	0.63	Flat chisel	Late Neolithic	Tisza
B12	74.44.15	Szerencs-Taktaföldvár	Y	Y	6.47	Flat chisel	Late Neolithic	Tisza
C02	53.206.3	Tiszadorogma	Y	Y	10.51	Flat chisel	Middle Neolithic	AVK
D02	70.1.149	Szerencs-Taktaföldvár	Y	Y	0.52	Flat chisel	Late Neolithic	Tisza
D04	58.42.2	Fancsal-farm	Y	Y	46.8	Flat chisel	Neolithic	Stray find
D05	not inventoried	Lidl Hejőkürt 2mh. S2106 2005. 06. 14.	Y	Y	1.69	Flat chisel	Middle Neolithic	AVK
D08	53.238.5	Szirmabesenyő's vicinity	Y	Y	17.17	Flat chisel	Middle Neolithic	Bükk AB, AVK
D12	53.248.1	Unknown	Y	Y	n.a.	Flat chisel	Neolithic	Stray find
D13	53.250.1	Bereg county	Y	N	0.68	Flat chisel	Neolithic	Stray find
D15	53.208.1	Emőd, Vaskó-sheer	Y	Y	0.62	Flat axe	Neolithic	Stray find
D17	74.44.11	Szerencs-Taktaföldvár	Y	Y	0.39	Flat chisel	Late Neolithic	Tisza
D18	not inventoried	Miskolc Aldi2 S153 2009. 09. 11.	Y	Y	24.33	Flat chisel	Middle Neolithic	AVK, Bükk
D21	53.160.20	Borsod/Derékegyháza (Edelény)	Y	Y	8.52	Shoe-last axe	Middle Neolithic	Bükk AB, B-C
D26	74.44.10	Szerencs-Taktaföldvár	N	Y	0.5	Flat chisel	Late Neolithic	Tisza
D30*	53.160.11	Borsod/Derékegyháza (Edelény)	Y	Y	1.69	Flat chisel	Middle Neolithic	Bükk AB, B-C
D31*	53.160.31a	Borsod/Derékegyháza (Edelény)	Y	N	1.44	Flat chisel	Middle Neolithic	Bükk AB, B-C
D32*	53.160.31b	Borsod/Derékegyháza (Edelény)	Y	Y	0.31	Shoe-last axe	Middle Neolithic	Bükk AB, B-C
Sample	Inventory number	Locality	EDS/SEM	PGAA	MS	Archaeological typology	Age	Culture/Phase
D33*	53.160.150	Borsod/Derékegyháza (Edelény)	Y	Y	29.62	Flat chisel	Middle Neolithic	Bükk AB, B-C
D34*	53.229.1	Muhi, Bala Hill	Y	Y	n.a.	Flat chisel	Neolithic	Unknown
D35	70.1.206	Szerencs-Taktaföldvár	N	Y	0.38	Axe fragment	Late Neolithic	Tisza
D37	67.13.3	Tolcsva's vicinity	N	Y	0.72	Flat axe	Neolithic	Unknown
D38	67.12.1	Egerlövő	N	Y	0.49	Shaft drilled axe	Neolithic	Unknown
D39	67.13.2	Tolcsva's vicinity	N	Y	n.a.	Shoe-last axe	Neolithic	Stray find
D40	53.187.3b	Hangács, Ludas Balk	N	Y	1.79	Shaft drilled axe	Neolithic	Unknown
D41	77.44.14	Szerencs-Taktaföldvár	N	Y	n.a.	Flat chisel	Late Neolithic	Tisza
D45*	72.11.303	Tiszavalk, Kenderföldek	Y	N	0.85	Flat chisel	Middle Neolithic	AVK
D47*	75.25.20	Unknown	Y	N	0.61	Flat chisel	Neolithic	Stray find
D48*	53.206.2	Tiszadorogma	Y	N	0.56	Tongue-shaped axe	Middle Neolithic	AVK

As regards the raw materials, amphibolite and amphibolite-greenschist stone tools are abundant implements in the Neolithic and Aeneolithic periods (Hovorka et al., 2001, Méres et al., 2001, Přichystal, 2013), being described as common and often used raw materials due to flexibility and elasticity of the ready-made items because of the needle-like of amphiboles (Hovorka et al., 2001).
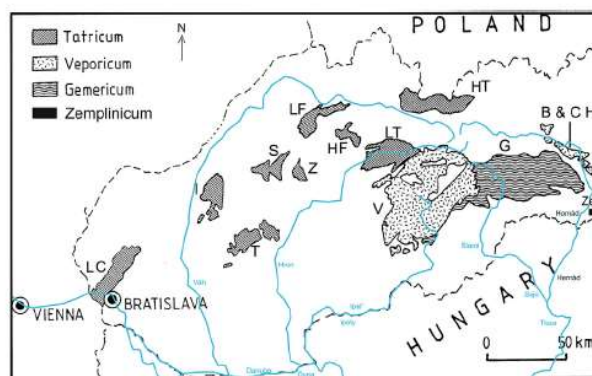

Fig. 2. Geographical setting of the main lithotectonic units containing amphibolite bodies of the Central-Western Carpathians and depicting the principal rivers of Slovakia. The schematic map is modified after Král' et al. (1997). Abbreviations on the map: B & CH: Branisko and Čierna Hora Mountains, G: Gemericum, V: Veporicum, LT: Low Tatras, HT: High Tatras, LF: Low Fatras, HF: High Fatras, S: Strážovské Mountains, Z: Žiar Mountains, I: Inovec Mountains, T: Tribeč Mountains, LC: Little Carpathians.

The most probable amphibolite source localities are not too far from the archaeological sites in the Western Carpathians. The Western Carpathians are defined by three major geological units: Veporicum, Gemericum and Tatricum (Plašienka et al., 1997). In the Veporicum, amphibolites are not dominant, but some large bodies are exposed in the Čierna Hora and the Branisko Mountains (Faryad, 1999, Faryad et al., 1999, 2005, Faryad & Jacko, 2002). Furthermore, the LAC (Leptynit-Amphibolite Complex) outcrops in Veľký Zelený stream and in Čierny Balog (Putiš et al., 1997). The Gneiss-

68 Amphibolite Complex (GAC) in the Gemericum has two main outcrops in Rudňany (Radvanec et al.,

69 2017) and in Klátov (Faryad, 1990, 1999, Faryad and Spišiak, 1999). The Ochtiná group is an exposure

70 of amphibolite rocks at the contact zone of Veporicum and Gemericum (Novotná et al., 2015). There

71 are only distant, minor occurrences in the Tatricum (Ivan et al., 2001). The most extensive outcrops

72 are in the Tribeč Mountains (Faryad, 1999) and Little Carpathians (Ivan et al., 2001). Zemplinicum is

73 the closest geological unit of the Carpathians to the archaeological localities; but here the amount of

74 amphibolites is much less than in the above regions (Faryad, 1995, Faryad and Vozárová, 1997). The

75 vicinities of major riverbeds of Slovakia which cross Hungary cannot be excluded as possible

76 provenance fields (Fig. 2).

77   In the southwestern part of Slovakia, at the Bajč archaeological site, a large number of polished

78 stone tools were excavated with various types of amphibolite and greenschist stone axes. According

79 to Hovorka and Cheben (1997), the possible provenance field of these amphibolites can be the Little

80 Carpathians, Slovak Ore Mountains, Tribeč Mountains, the eastern part of the Bohemian Massif,

81 Eastern/Northern Alps and also pebbles of the Hron and Danube riverbeds.

82   In this research we provide petrological and mineralogical data of the Neolithic amphibolite

83 implements and compare them with the former published data of nearby Slovakian amphibolite source

84 localities and specification of the most probable provenance of the raw material.

85

86 **2. Analytical techniques and materials**

87   In addition to macroscopic and stereomicroscopic descriptions, the magnetic susceptibilities

88 of all the axes were measured by a KT-5 Kappameter, using thickness correction (Bradák et al., 2009,

89 Szakmány et al., 2011b, Kereskényi et al., 2015 a, b.).

90   Non-destructive methods were applied since most of the implements are intact. While

91 destructive analyses were performed only on some broken stone implements (Table 1).

92   The chemical elements in the bulk material of 24 polished archaeological stone objects (Table

93 1) have been measured by the prompt-gamma activation analysis (PGAA) system of the Budapest

94 Neutron Centre. The present state of the PGAA facility in Budapest was described by Szentmiklósi et

95 al. (2010) in detail. During the analysis, the entire objects were placed in a horizontal beam of cold

96 neutrons guided from the Reactor. The flux of the cold neutron beam equivalent to the thermal beam

97 was 1.2×10^8 neutrons cm^{-2} s^{-1}. During the experiments, the beam was setup to 24 mm^2 and 44 mm^2

98 size cross-section. With such beam collimation, the obtained count rate proved to be optimal from

99 spectroscopic points. Since neutrons can travel into the deepest parts of the investigated object, the

100 obtained composition data represents the bulk. Promptly after the neutron absorption, characteristic

101 gamma radiation is emitted, which was detected with a HPGe-BGO detector system. The spectra were

102 collected with a 36,000-channel analyser. To identify characteristic gamma lines, our PGAA library has

103   been used. The quantitative elemental compositions have been calculated based on the k_0-method

104   (Révay, 2009). In silicates, the PGAA method allows to determine all the major elements and some

105   geochemically important traces (such as B, Cl, Sc, V, Cr, Co, Nd, Sm and Gd), non-destructively, see

106   Kasztovszky et al. (2008), Szakmány and Kasztovszky (2004), and Szakmány et al. (2011a). In these

107   experiments, the spectrum acquisition has been performed for 1200 s -3000 s, to gain enough counts

108   in the relevant spectrum peaks to produce statistically reliable results.

109

110   Quantitative chemical spot analyses on the mineral phases were performed applying a JEOL

111   JXA 8600 Superprobe electron-microprobe in energy-dispersive mode (EDS/SEM) at the Institute of

112   Mineralogy and Geology, University of Miskolc. The operating conditions were as follows: accelerating

113   voltage 15 kV, probe current 20 nA, and a 1-5 μm beam diameter. The intact tools were analysed on

114   their original surfaces using the method of Bendő et al. (2013), while polished surface sections were

115   made from the broken implements for their analyses (Table 1).

116

117   **3. Results**

118   *3.1. Macroscopic description and magnetic susceptibility*

119   Most of the stone implements are intact and having traces of use. They are 4.0-11.5 cm long,

120   1.0-6.5 cm wide and 0.5-4.0 cm thick. Regarding their archaeological typology, most of them are flat

121   axes and chisels, but axes D21, D32, D39 have shoe-last form, D38 and D40 are shaft drilled stone axes,

122   and D48 is a tongue-shaped axe.

123   Macroscopically the tools are fine-grained, compact, dominantly foliated, having grey, greyish

124   black, greyish green and dark brown colour. Green and brown patches and bands can be recognized

125   by naked eye.

126   Magnetic susceptibility values show a homogenous distribution from $0.31\text{-}0.85*10^{-3}$ SI. 4

127   samples appear from $1.44\text{-}1.77*10^{-3}$ SI and sporadically a continuous upward from 6.47 to $46.7*10^{-3}$ SI

128   (Table 1).

129

130   *3.2. Bulk rock chemistry*

131   Bulk compositional data analysed by PGAA for the amphibolite implements are listed in Table

132   2. The tools are characterized by SiO_2 content ranging from 46.55 to 59.00 wt%. Sample D12 has an

133   elevated TiO_2 content= 3.70 wt% and remarkably differs in some of the trace elements from the other

134   analysed samples. Representing the data in a TAS diagram, the analysed samples plot in the basalt,

135   trachybasalt, basaltic andesite and andesite fields, having subalkaline characteristics since the

136   Na_2O+K_2O content varies between 0.92-5.17 wt%. (Fig. 3). In the AFM diagram most of the samples

137   show tholeiitic affinity (Fig. 4).

138

139   *3.3. Petrography and mineral chemistry*

140   A total of 22 polished stone tools were analysed by EDS/SEM. Eight of them are intact stone

141   axes and were analysed by the "original surface" method (Bendő et al., 2013). In these cases, the zoned

142   mineralogical features (e.g. the existence of tiny or scarce phases) the zonation of the amphiboles

143   could not always be perceived.

Table 2

PGAA results. The major components are given in wt%, the trace elements are in ppm. The amount of oxides is calculated from the elemental concentration, based on the oxidation numbers. The number of digits indicates the uncertainties of concentration values. " < D.L." stands for "less than the Detection Limit".

Sample	B04	B05	B12	C02	D02	D04	D05	D08	D12	D15	D17	D18
SiO_2	54.18	50.39	47.77	47.85	47.00	49.00	50.00	50.00	50.00	47.00	59.00	52.00
TiO_2	0.46	2.28	2.29	2.63	1.61	1.53	1.92	1.48	3.70	1.29	1.07	1.70
Al_2O_3	13.58	16.11	14.36	15.04	13.00	13.50	15.50	13.60	13.00	15.00	17.80	13.90
$Fe_2O_3^*$	10.07	12.53	12.71	13.13	11.70	12.40	9.60	12.30	13.20	10.70	5.40	11.20
MnO	0.21	0.17	0.18	0.24	0.23	0.21	0.23	0.26	0.18	0.28	0.10	0.17
MgO	5.76	5.47	7.06	4.95	7.40	3.50	6.30	7.90	5.60	7.80	3.00	6.90
CaO	7.48	4.74	8.30	9.32	13.10	11.80	10.90	12.10	9.80	14.90	7.20	8.80
Na_2O	4.12	4.70	3.52	3.50	1.30	1.30	2.27	1.53	2.50	0.73	2.97	3.15
K_2O	1.04	0.38	1.47	0.86	0.13	0.18	0.25	0.12	< D.L.	0.19	1.17	0.24
H_2O	1.59	3.16	2.22	2.27	1.69	1.72	1.59	1.62	1.21	1.63	2.24	1.30
SO_3	1.38	< D.L.	< D.L.	< D.L.	2.60	1.22	1.72	0.43	0.48	< D.L.	< D.L.	0.41
Total	99.90	99.92	99.89	99.76	99.76	96.36	100.28	101.34	99.67	99.52	99.95	99.77
B	10	1	2	1	6	3	4	3	2	12	20	3
Cl	407	305	689	798	196	200	220	290	23	270	105	180
Sc	< D.L.	39	< D.L.	65	53	40	101	51	< D.L.	29	23	12
V	134	234	185	409	480	310	670	340	390	170	160	230
Cr	< D.L.	< D.L.	< D.L.	506	< D.L.	< D.L.	< D.L.	< D.L.	< D.L.	< D.L.	< D.L.	< D.L.
Co	< D.L.	< D.L.	< D.L.	< D.L.	< D.L.	< D.L.	< D.L.	< D.L.	< D.L.	< D.L.	< D.L.	< D.L.
Nd	< D.L.	< D.L.	29	< D.L.	15	< D.L.	21	33	34	21	22	17
Sm	1	4	4	5	2	2	3	2	6	2	3	5
Gd	2	6	5	7	4	4	5	4	7	3	4	7

Sample	D21	D26	D30	D32	D33	D34	D35	D37	D38	D39	D40	D41
SiO_2	47.00	53.00	50.00	49.00	52.80	48.00	46.55	56.22	50.00	52.00	47.00	51.00
TiO_2	1.71	1.41	2.06	1.78	2.19	1.32	1.39	1.08	0.82	1.10	2.50	2.12
Al_2O_3	13.60	13.20	15.11	14.80	13.64	13.80	15.78	18.11	15.60	11.20	12.90	15.30
$Fe_2O_3^*$	11.40	8.50	11.10	10.20	11.75	11.10	11.85	5.96	9.70	12.50	12.60	10.90
MnO	0.19	0.28	0.17	0.19	0.20	0.20	0.22	0.14	0.10	0.34	0.39	0.19
MgO	7.30	7.20	7.60	6.50	5.90	7.40	8.94	3.39	6.60	7.10	6.20	4.20
CaO	10.30	11.40	7.40	12.70	7.77	14.70	9.96	8.79	12.40	13.00	11.20	9.20
Na_2O	1.63	2.80	4.30	1.87	3.76	1.78	2.84	3.04	2.20	0.81	2.05	3.90
K_2O	0.16	0.32	0.33	0.16	0.42	0.25	0.44	1.00	0.28	0.40	0.31	0.82
H_2O	1.59	1.30	1.68	1.67	0.97	1.66	1.94	2.24	1.89	1.49	2.21	2.30
SO_3	5.00	0.59	0.64	1.28	0.53	< D.L.	< D.L.	< D.L.	< D.L.	0.31	2.70	< D.L.
Total	99.88	101.89	100.38	100.15	99.93	100.21	99.93	99.97	99.59	100.25	100.06	99.93
B	4	4	3	3	4	6	5	23	6	4	7	2
Cl	200	201	42	250	190	0	< D.L.	90	510	570	290	690
Sc	47	33	< D.L.	65	< D.L.	< D.L.	46	34	19	9	44	21
V	410	250	360	268	360	336	< D.L.	250	310	430	270
Cr	< D.L.	< D.L.	< D.L.	< D.L.	< D.L.	< D.L.	< D.L.	< D.L.	< D.L.	< D.L.	< D.L.	< D.L.
Co	< D.L.	< D.L.	< D.L.	< D.L.	< D.L.	< D.L.	< D.L.	< D.L.	< D.L.	< D.L.	< D.L.	< D.L.
Nd	14	21	32	19	< D.L.	80	< D.L.	22	230	20	16	30
Sm	3	3	4	3	7	2	3	4	1	2	4	3
Gd	4	4	7	5	10	4	5	5	2	3	5	4

*Total Fe as Fe_2O_3.

144

145   Most of the stone implements are fine-grained, but some stone tools (D08, D12, D13, D15, D18

146   and D30 are coarse-grained (Figs. 5 A—D, 6 A—C). Most of the axes are foliated (Figs. 7 A—D) except

147   B04, B05, B12, D17, D18, D33, D45 and D47 samples.

148   The amphibolites consist mainly of Ca-amphibole (Mg-hb, Act, Tsch, Prg, Sdg), plagioclase,

149   epidote, clinozoisite, chlorite and quartz. Some samples contain clinopyroxene, K-feldspar, biotite in

150   minor quantity. Titanite and ilmenite are abundant accessory minerals (Table 3).

151   According to the textural relations, chemical compositions and the assemblage of coexisting

152   phases, two varieties of the detected stone implements can be distinguished. The first variety (*Group1*)

153   includes six samples and it consists of Ca-amphiboles with increasing Al(tot) content from cores to

154   rims. Actinolite and magnesio-hornblende are preserved in the cores with Al(tot) 0.14-2.84 apfu

155   (atoms per formula unit), while at the rims magnesio-hornblende, pargasite and tschermakite have

156   crystallized with Al(tot) 0.73-2.83 apfu (Fig. 8).

157   The second group (*Group2*) includes 16 pieces of stone tools and their amphibole content

158   corresponds to hornblende, pargasite, tschermakite and sadanagaite in the core with actinolite at the

159   rims, just the opposite of the order in Group1 tools. Group2 was divided into four subgroups based on

160   mineral associations:

161   -   *Group2a* includes most of the implements in which no K-feldspar or biotite were detected

162   (B12, D02, D04, D08, D18, D21, D32, D47),

163   -   K-feldspar±biotite-bearing amphibolites (*Group2b*: B04, B05, C02, D48),

164   -   Clinopyroxene±biotite-bearing amphibolites (*Group2c*: D15, D34, D45),

165   -   Biotite-bearing amphibolite without K-feldspar and clinopyroxene (*Group2d*: D17).

166

167   *3.3.1. Amphibole*

168   The ACES Excel spreadsheet was used to calculate cation numbers of amphiboles. Since the

169   Fe^{3+}/Fe(tot) ratio cannot be measured by electron-microprobe, the smallest maximum deviations

170   criteria were applied for adjusting the valences of Fe by automatically selecting one or more of four

171   cation normalization schemes: sum Si to Ca (+Li) = 15; sum Si to Mg (+Li) = 13; sum Si to Na = 15; and

172   sum Si to K = 16 apfu (Locock, 2014). Applied amphibole nomenclature corresponds to the recent IMA

173   rules (Hawthorne et al., 2012).
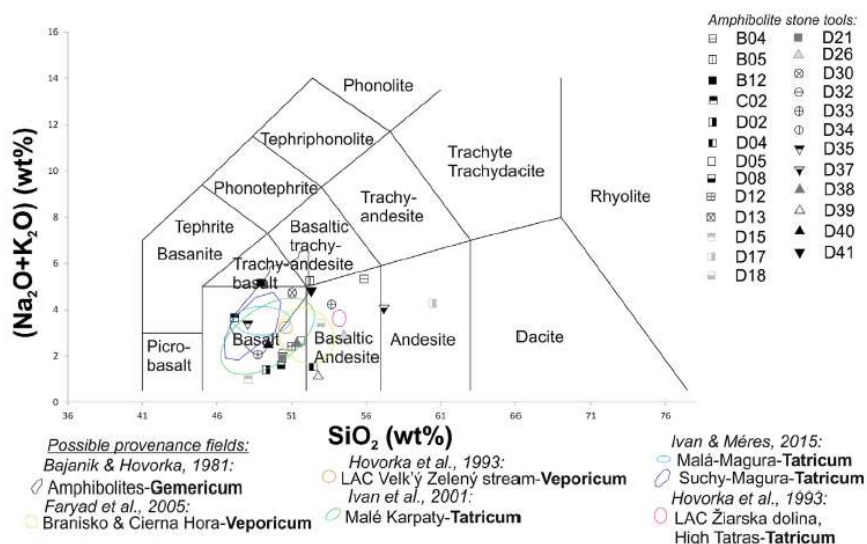

Fig. 3. Amphibolite implements from the Herman Ottó Museum and their potential provenances plotted in the Total Alkali- Silica (TAS) diagram.

174

175   *Group1*

176   In each detected commonly zoned Ca-amphibole of the *Group1* variety, the ^{B}Na/(Ca+Na) varies

177   in a narrow range of 0.00-0.19 both in the cores and rims. Overlapping ^{A}Na and X_{Mg} values characterize

178   amphiboles in the cores and at the rims. [A]Na ranges over 0.00-0.65 apfu and X_{Mg} is fairly homogenous

179   with values of 0.49-0.79.

180   Actinolite with [IV]Al 0.12-0.44, [VI]Al 0.01-0.65 and Al(tot) 0.14-1.03 apfu was detected in the

181   cores of all samples except D30. Magnesio-hornblende occurs in the cores of the D05, D30 and D31

182   samples with [IV]Al 0.33-1.13, [VI]Al 0.50-1.71, Al(tot) 0.44-2.84 apfu. In the D05, D12, D13 and D33

183   samples, magnesio-hornblende–magnesio-ferri-hornblende with [IV]Al 0.28-1.12, [VI]Al 0.60-1.64 and

184   Al(tot) 0.73-2.75 apfu makes a rim of actinolite-magnesio-hornblende (Fig. 5 B, D). Tschermakite was

185   detected at the rims of earlier crystallized amphiboles in D05, D30 and D31 samples with [IV]Al 1.10-1.48,

186   [VI]Al 1.15-1.55 and Al(tot) 2.50-2.63. Pargasite with [IV]Al 0.72-1.13, [VI]Al 1.52-1.70, Al(tot) 2.31-2.83 apfu

187   was described from the rims on the actinolite–magnesio-hornblende in the D30 and D31 samples.

188   *Group2*

189   In *Group2* the [A]Na values are 0.00-0.60 apfu, [B]Na/(Ca+Na) ranges from 0.00 to 0.19 and X_{Mg} is

190   0.30-0.79, values which overlap in the cores and rims.

191   Generally, in *Group2a* (Figs. 6 G—I, Fig. 7 D) most of the samples have a magnesio-hornblende core

192   with [IV]Al 0.01-0.93, [VI]Al 0.07-1.79, Al(tot) 0.84-2.29 apfu, and actinolite–hornblende was observed with

193   [IV]Al 0.18-0.54, [VI]Al 0.00-0.50, Al(tot) 0.23-0.89 apfu at the rims. Ferri-tschermakite and ferro-ferri-

194   tschermakite were determined for the core of sample D08 (Fig. 7 C—D) with Al(tot) 2.13 apfu. In the

195   core of the D47 stone implement pargasite–ferropargasite prevail with Al(tot) 2.64-3.31 apfu in

196   addition to magnesio-hornblende. In the core of the B12 tool pargasite, ferropargasite, sadanagaite

197   and ferrosadanagaite (Fig. 6—I) are present with an increased Al(tot) from 2.97 to 3.45 apfu.
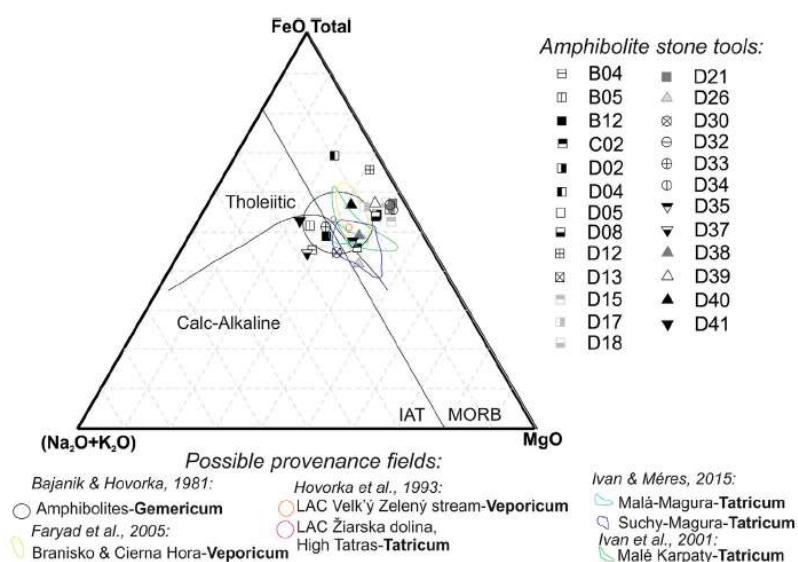

Fig. 4. AFM diagram of the investigated amphibolite implements and their possible fields of amphibolite localities plotted in AFM (Irvine and Baragar, 1971) diagram. A = alkali (Na₂O + K₂O), F = FeO (total), M = MgO. IAT = island arc tholeiite, MORB = mid-ocean ridge basalt.
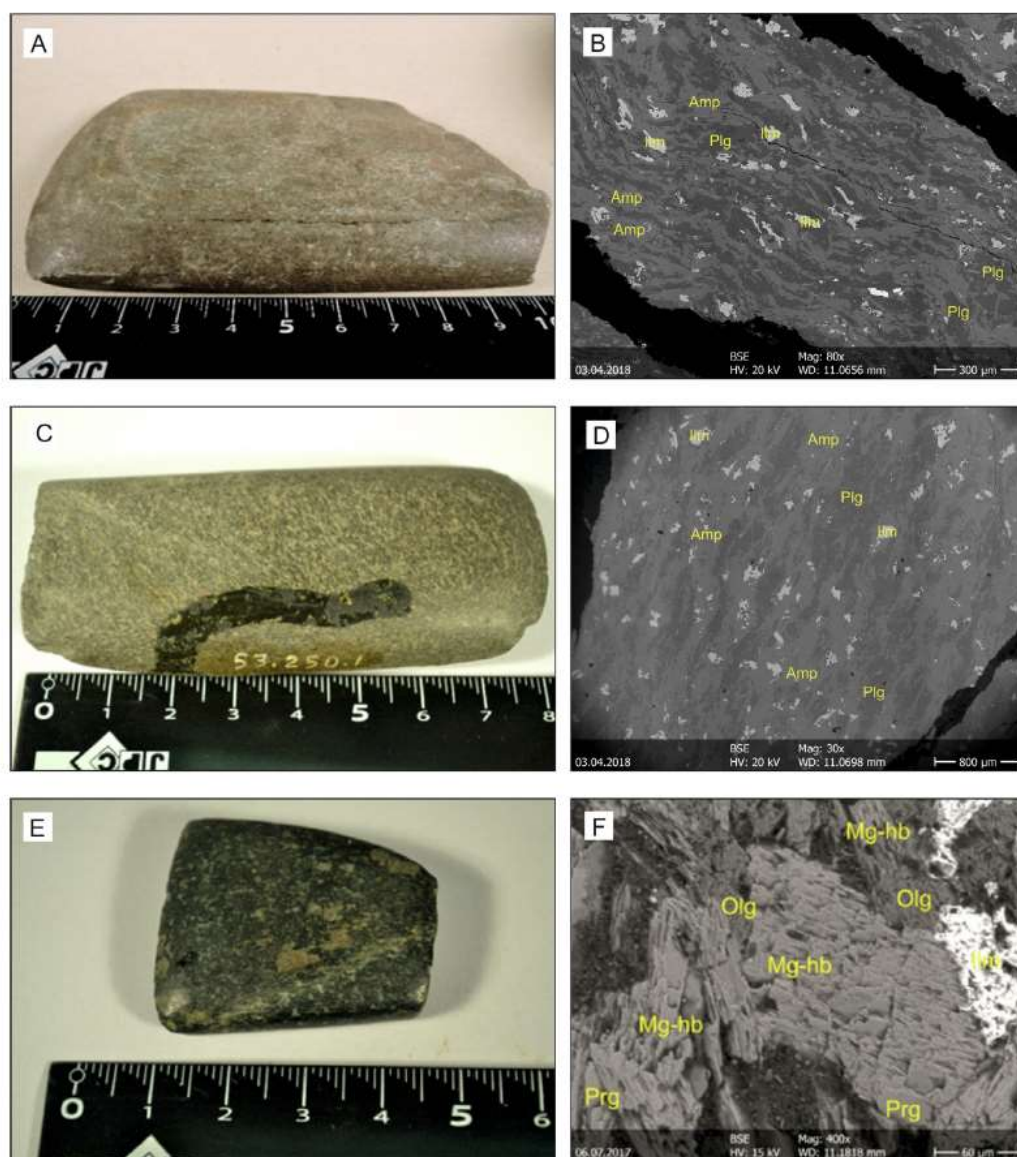
198

199

Fig. 5. A, B Macroscopic and BSE images of the coarse-grained sample D12 (*Group1a*). C, D Macroscopic and BSE images of the coarse-grained sample D13 (*Group1a*). E, F Macroscopic and BSE images of sample D30 (analysed by original surface) (*Group1b*).

200

201 In *Group2b* most of the samples have magnesio-hornblende–ferro-hornblende cores, although

202 in D48 pargasite and ferro-pargasite were detected also. The amphibole cores have ranges of ^{IV}Al 0.41-

203 0.75, ^{VI}Al 0.39-1.40, Al(tot) 0.86-2.00 apfu, while at the actinolite rims a significant decrease shows up,

204 with ranges of ^{IV}Al 0.23-0.48, ^{VI}Al 0-0.42, Al(tot) 0.36-0.66 apfu.

205 In *Group2c* magnesio-hornblende–ferro-hornblende cores were recorded having ^{IV}Al 0.30-

206 0.92, ^{VI}Al 0.60-1.30, Al(tot) 0.83-2.21 apfu and at the rims magnesio-hornblende–actinolite were

207 observed with ^{IV}Al 0.07-0.35, ^{VI}Al 0.27-0.64, Al(tot) 0.52-1.03 apfu.

208 *Group2d* consists of only the D17 implement, in which magnesio-hornblende–ferropargasite

209 exists in the core with ^{IV}Al 0.35-1.03, ^{VI}Al 0.39-1.68 Al(tot) 0.86-2.73 apfu and with magnesio-

210 hornblende–actinolite rimming the earlier crystallized amphiboles with ^{IV}Al 0.13-0.42, ^{VI}Al 0.05-0.43,

211 Al(tot) 0.18-0.76 apfu.

212   Chemical compositions of the calcic amphiboles are presented in Tables 4, 5.

213   The detected amphiboles of the amphibolites of *Group1* and *Group2* lie in the actinolite,

214   magnesio-hornblende, tschermakite, pargasite, and sadanagaite fields (Figs. 8, 9) in the ^{A}(Na+K+2Ca)

215   vs ^{C}(Al+Fe^{3+}+2Ti) diagrams.

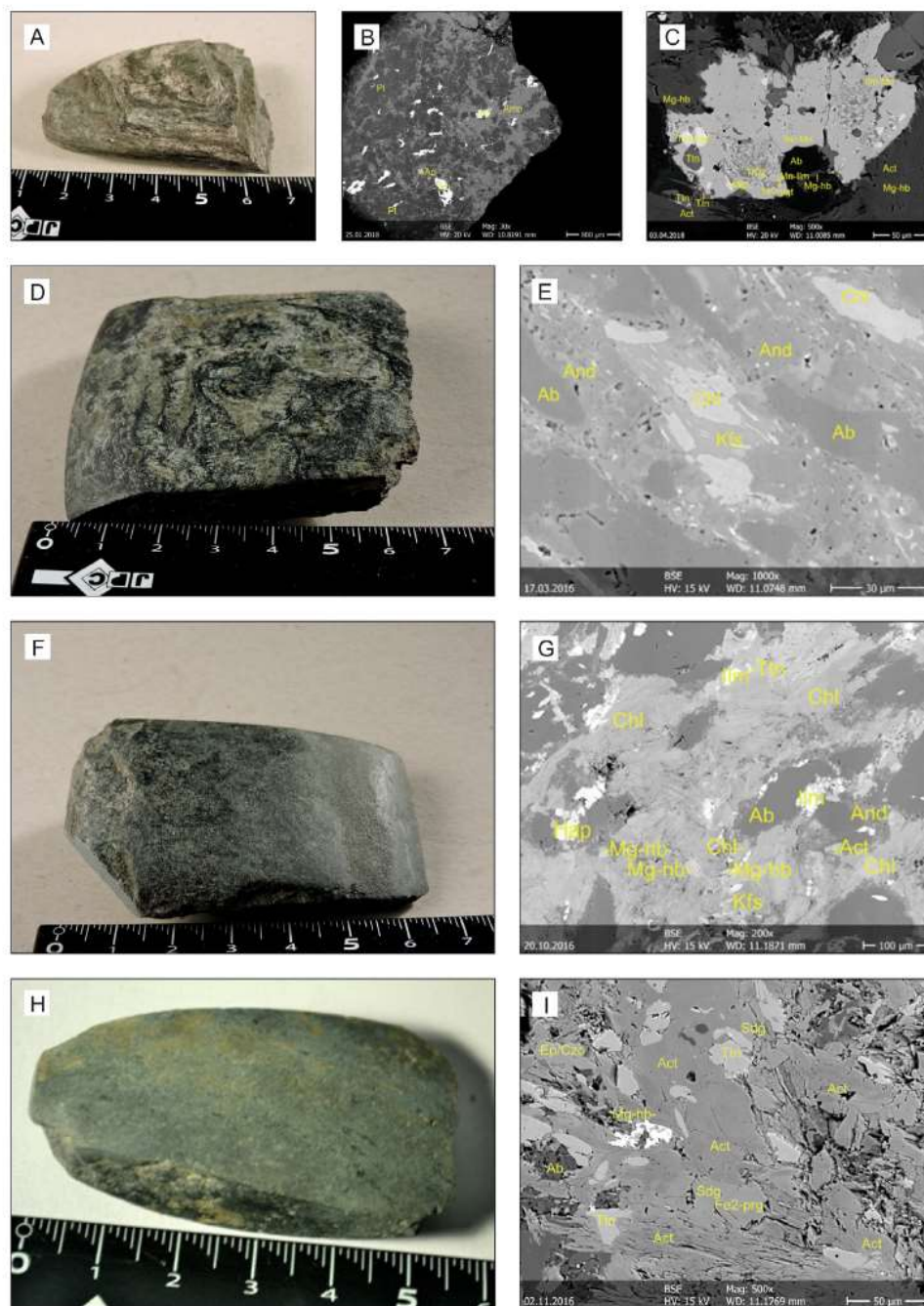**Fig. 6.** A, B Macroscopic and BSE images of the coarse-grained, ilmenite-rich sample D18 (*Group2a*). C – Ilmenite is partly replaced by titanite with magnetite inclusions in the BSE image of the sample D18. D, E Macroscopic and BSE images of the sample B04 (*Group2b*). F, G Macroscopic and BSE images of the sample B05 (*Group2b*). H, I Macroscopic and BSE images of the sample B12 (*Group2a*).

216

217   *3.3.2 Pyroxenes*

218   The pyroxene formula was calculated on the basis of 6 oxygens. The FeO/Fe_2O_3 ratio was

219   estimated assuming a total number of cations of 4. Normalized pyroxene end members found in

220   amphibolites are plotted in the En-Fs-Wo diagram (Fig. 10) of Morimoto (1989). *Augite* forms

221   hypidioblasts and xenoblasts as a relict phase next to actinolite and hornblende in small amounts in

222   the D34 ($En_{0.37}$ $Fs_{0.28}$ $Wo_{0.34}$) and D45 samples ($En_{0.28-0.39}$ $Fs_{0.25-0.50}$ $Wo_{0.23-0.42}$). *Diopside* is observed as a

223   relict phase in the D15 sample. Its chemical composition varies in a narrow range $En_{0.38-0.39}$ $Fs_{0.15}$ $Wo_{0.47}$.
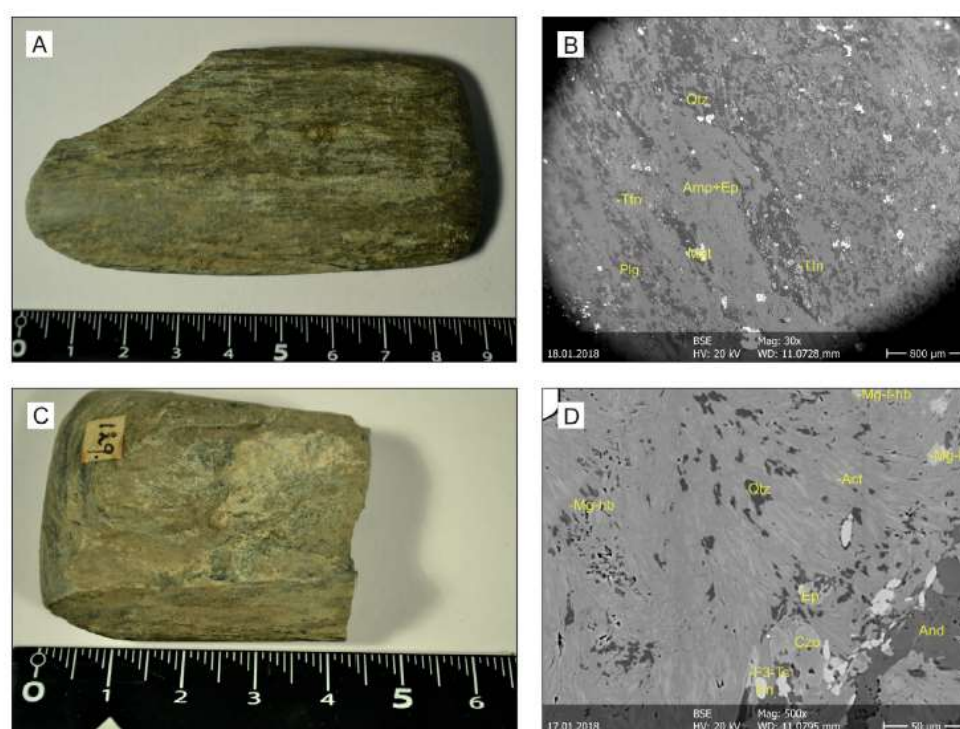

Fig. 7. A, B Macroscopic and BSE images of the foliated, epidote-rich D04 sample (*Group2a*). C, D Macroscopic and BSE images of the well-foliated D08 sample (*Group2a*).

224

Table 3
Main diagnostic minerals of *Groups- 1* and *2* of amphibolite stone implements.

Sample	Amphibole		Plagioclase		Kfs	Bi	Ep/Czo	Cpx
Group1	core	rim	Pl1 (core)	Pl2 (rim)				
D05	Act; Mg-hb	Mg-hb; Tsch	Lab	And				
D12	Act	Mg-hb	Ab	And				
D13	Act	Mg-hb	Lab	And				
D30	Mg-hb	Tsch; Prg	Ab	Olg				
D31	Act; Mg-hb	Tsch; Prg	And, Olg	And, Olg				
D33	Act	Mg-hb; Mg-f-hb	Ab	Olg			X	
Group2								
Group2a								
B12	Sdg; Fsdg; Prg; Fprg	Mg-hb; Act	And	Ab			X	
D02	Mg-hb; Fhb	Act; Fact	Lab, And, Olg	Ab			X	
D04	Mg-hb	Mg-hb	Lab, And	Lab, And			X	
D08	Mg-hb; Mg-f-hb; Fe2-ftsch; Fe3-Ts	Act	Lab, And	Lab, And			X	
D18	Mg-hb	Act	Lab, And, Olg	Ab				
D21	Mg-f-hb	Mg-f-hb	Byt, And	Ab				
D32	Mg-hb	Act	And, Olg	Ab				
D47	Mg-hb; Prg; Fprg	Act	And	Ab			X	
Group2b								
B04	Mg-hb	Act	And, Olg	Ab	X			
B05	Mg-hb	Act; Fact	Lab, And	Ab	X			
C02	Fhb, Mg-hb	Fhb, Act	Byt	And, Olg	X	X		
D48	Fprg, Mg-hb	Fprg, Mg-hb	And, Lab	And, Lab	X		X	
Group2c								
D15	Mg-hb	Act	Byt, Lab	And	X	X	X	X
D34	Mg-hb	Mg-hb; Act	And	Ab				X
D45	Fhb	Act	Lab; And	Lab; And				X
Group2d								
D17	Fprg; Mg-hb	Mg-hb; Act	And, Olg	Ab		X	X	
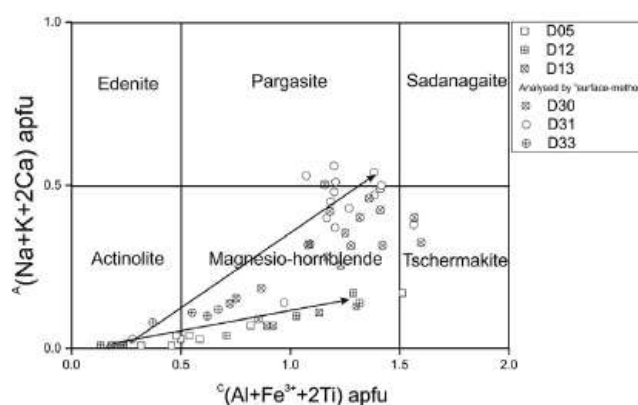
Fig. 8. Chemical composition of calcic amphiboles of *Group1* amphibolites plotted in the $^{C}(Al + Fe^{3+} + 2Ti)$ vs $^{A}(Na + K + 2Ca)$ diagram. Arrows indicate the phase changes from core to rim.

3.3.3 Feldspars

Plagioclase shows various chemical compositions from albite to bytownite in the amphibolites (Fig. 11).

In the D31 sample of *Group1*, the textural relations or core to rim zoning of the plagioclases was not well distinguished due to the limitations of the "original surface" method. Its composition varies from oligoclase to andesine with $An_{23.0-30.0}$. In the D05 and D13 stone axes, a labradorite composition with a narrow range of $An_{54.3-61.9}$ is present in the core (Pl1), presumably as a relict magmatic phase, while at the rim (Pl2) it is andesine with $An_{47.1-49.9}$ (Table 3). In the D12, D30 and D33

238 stone implements, albite ($An_{0.0-6.7}$) is the pre-kinematic plagioclase (Pl1) (Table 3). In samples D30 and

239 D33, oligoclase ($An_{15.9-29.6}$) (Fig. 11), and in the D12 sample andesine ($An_{37.9-44.5}$) are the post-kinematic

240 phases (Pl2) (Table 3).

241   In samples D04, D08, D45 and D48 of *Group2*, it was not possible to define the textural

242 relations of plagioclases with andesine ($An_{40.3-49.5}$) and labradorite ($An_{50.9-64.8}$) compositions. In the

243 stone implements C02 and D15, plagioclase of labradorite and bytownite composition ($An_{63.1-89.0}$) is a

244 relict phase (Pl1) while oligoclase-andesine ($An_{13.4-46.5}$) is the typical composition for the rim (Pl2). For

245 the other samples of *Group2*, the relict phases have values of $An_{24.4-65.7}$ for Pl1 and the post-kinematic

246 minerals were albite, described with $An_{0.0-9.1}$ content as Pl2 (Table 3, Figs. 6—E, G, I). Potassic feldspar,

247 as a relict phase is detected in *Group2b* (Figs. 6—E, G).

248 *3.3.4 Other minerals*

249   *Epidote/clinozoisite* is present in 9 samples (Table 6). Epidote/clinozoisite is mainly zoned,

250 where Fe-content increases from the core to rim. In the D02 and D04 tools the amount of epidote and

251 clinozoisite reaches 30 vol% (Fig. 7—B). *Biotite* was identified in tools C02, D15, and D17 (*Group2*). In

252 samples C02 and D17, biotite is partially replaced by chlorite. Biotite occurs up to 50 µm in diameter.

253 Its chemical compositions are listed in Table 7. *Ilmenite* forms idioblastic and hypidioblastic grains. In

254 the samples B12 (Fig. 6—I), D15 and D18 (Fig. 6—C) ilmenite is partly replaced by titanite and contains

255 magnetite and Ti-bearing magnetite as inclusions. MnO content in ilmenite from samples B12, D05 and

256 D18 reaches 3.00-3.97 wt%. In sample D18 the size of ilmenite tablets reaches 600 µm in diameter.

257 *Titanite* is a common accessory mineral and was found in nearly all the tools except B05, D13, D31 and

258 D33. Its Al_2O_3 content is typically high, varying in the range of 1.26-5.79 wt%. The highest value was

259 recorded in the D05 sample but shows elevated values (2.28-4.01 wt%) in the B04, D15, D18 and D45

260 samples as well.

261   *Magnetite* is observed in the D04, D18, D21 and D33 samples. In D04 it is distributed along

262 foliations with grain size up to 200 µm (Fig. 7—B). In tool D18, magnetite and Ti-bearing magnetite

263 (TiO_2: 4.29 wt%) is recognized as inclusions in Mn-bearing ilmenite (Fig. 6—C). *Chlorite* was observed

264 in five samples. In sample D13, chlorite of clinochlore composition is present at the contact of actinolite

265 and epidote. In tool D02 it was observed at the rim of magnesio-hornblende. In sample D04, chlorite

266 developed inside hematite and both in D02 and D04 samples chlorite was identified as chamosite. The

267 chemical compositions of the chlorites are presented in Table 8.

268

269 **4. Discussion**

270 *4.1 Thermobarometric estimations*

271   As no garnet was found in the studied samples, the application of thermobarometric methods

272   was limited. Since amphibole is a common mineral present in all amphibolite polished stone tools, the

273   single Ca-amphibole approach of Gerya et al. (1997) was applied to calculate peak pressure and

274   temperature ($P_{(Tmax)}$-T_{max}) conditions. The method was modified for Fe^{3+} by Zenk & Schulz (2004). Based

275   on their suggestion, the 13CNK method (Locock, 2014) was used to determine the amphibole formulae.

276   In this method, the absolute errors of the calculation are generally reduced to ±1.2 kbar and ±37 °C.

277   *Group1*

278   In sample D33, the magnesio-hornblende in the rim implies T_{max} 460 °C and $P_{(Tmax)}$ 2.8 kbar. In

279   the D05 sample, tschermakite which rims magnesio-hornblende crystallized at 540 °C and 5.3 kbar.

280   The D12 and D13 samples have very similar mineral assemblages and their P-T data calculated from

281   magnesio-hornblende in the rim yield T_{max} of 560–570 °C and $P_{(Tmax)}$ of 5 kbar. Tschermakite in the rim

282   (Table 3) in D30 and D31 samples implies T_{max} 615–635 °C and 5–6 kbar for $P_{(Tmax)}$. In D30, pargasite

283   which rims magnesio-hornblende yielded T_{max} of 615 °C and 5.6 kbar for $P_{(Tmax)}$ (Table 9). In the D31

284   sample, the pargasite rim (Table 3) crystallized at 635 °C and 6.2 kbar and the magnesio-hornblende

285   core (Table 3) yields the same P-T data (Table 9, Fig. 12).

286

287   *Group2*

288   In sample D08 of *Group2a*, tschermakite occuring along with magnesio-hornblende yielded

289   600 °C and 4.8 kbar in Table 9. In sample B12, the core pargasite recorded 670 °C and 6.5 kbar, the

290   core sadanagaite yields similar data of 680 °C and 7.3 kbar. In the D47 sample, core pargasite

291   crystallization recorded 690 °C and 7.0 kbar. In the D48 sample (*Group2b*), ferro-pargasite

292   crystallization yielded T_{max}: 590 °C and $P_{(Tmax)}$ 4.6 kbar. In sample D17 of *Group2d*, ferro-pargasite

293   rimmed by actinolite reached 610 °C and 5.7 kbar. In the other samples *of Group2*, the peak

294   metamorphism was determined from magnesio-hornblende with T_{max} of 450–610 °C and $P_{(Tmax)}$ of 2.8–

295   5.7 kbar (Table 9).

296   Plotting the T_{max} versus the $P_{(Tmax)}$ values, a continuous transition of simultaneously increasing

297   values in the medium-temperature- and high-temperature fields can be observed (Table 9, Fig. 12).

298   The medium-temperature group presents T_{max} ≈550 °C and $P_{(Tmax)}$ ≈5.3 kbar. For the high-temperature

299   group, in which tschermakite-, pargasite-bearing amphibolite implements are present, the thermal

300   maximum, T_{max} ≈600 °C and $P_{(Tmax)}$ 5–6 kbar are characteristic. The sadanagaite-bearing sample (B12)

301   and a pargasite-bearing sample (D47) reached the highest peak temperatures. The B12 sample

302   suggests T_{max} of 680 °C and $P_{(Tmax)}$ of 7.3 kbar and the D47 sample yields T_{max} of 690 °C and $P_{(Tmax)}$ of 7.0

303   kbar (Table 9, Fig. 12).

304   The tools in *Group2* were overprinted by greenschist facies metamorphism as magnesio-

305   hornblende and actinolite surrounding earlier crystallized Ca-amphiboles.

306   The results of the thermobarometric calculations are listed in Table 9 and plotted in Fig. 12.

Table 4
Chemical composition of amphiboles (*Group 1*).

No.	1	2	3	4	5	6	7	8
Sample	D05-15	D30	D30	D31	D30	D30	D31	D31
SiO_2	47.83	45.05	45.71	44.21	44.32	44.45	43.47	43.48
TiO_2	0.16	0.35	0.30	0.26	0.30	0.40	0.45	0.50
Al_2O_3	15.60	15.68	15.09	16.54	13.94	13.45	16.53	14.88
MnO	0.23	0.00	0.00	0.11	0.05	0.00	0.10	0.19
FeO*	12.60	9.14	9.12	10.40	12.34	14.51	11.44	12.54
Fe_2O_3*	0.00	3.66	4.04	2.93	2.10	0.00	1.45	1.60
MgO	8.80	12.21	11.56	10.65	11.48	11.62	10.91	10.98
CaO	10.80	8.82	9.16	10.28	11.15	11.29	10.88	11.63
Na_2O	1.64	2.76	2.63	2.34	2.06	1.97	2.58	1.88
K_2O	0.32	0.28	0.34	0.25	0.24	0.29	0.17	0.31
H_2O**	2.05	2.04	2.04	2.03	2.00	2.01	2.03	2.01
Total	100.00	100.00	100.00	100.00	100.00	100.00	100.00	100.00
Cation numbers based on 23 oxygens								
Si	6.85	6.45	6.55	6.38	6.46	6.48	6.30	6.36
Al	1.15	1.55	1.45	1.62	1.54	1.52	1.70	1.64
ΣT	8.00	8.00	8.00	8.00	8.00	8.00	8.00	8.00
Ti	0.02	0.04	0.03	0.03	0.03	0.04	0.05	0.06
Al	1.48	1.10	1.10	1.19	0.86	0.79	1.13	0.92
Fe^{3+}	0.00	0.40	0.44	0.32	0.23	0.23	0.16	0.18
Mn^{2+}	0.03	0.00	0.00	0.00	0.00	0.00	0.00	0.00
Fe^{2+}	1.51	0.87	0.97	1.18	1.38	1.40	1.31	1.46
Mg	1.88	2.61	2.47	2.29	2.50	2.53	2.36	2.39
ΣC	4.91	5.00	5.00	5.00	5.00	5.00	5.00	5.00
Mn^{2+}	0.00	0.00	0.00	0.01	0.01	0.00	0.01	0.02
Fe^{2+}	0.00	0.23	0.13	0.08	0.13	0.13	0.08	0.08
Ca	1.66	1.35	1.41	1.59	1.74	1.76	1.69	1.82
Na	0.34	0.42	0.47	0.32	0.13	0.10	0.22	0.08
ΣB	2.00	2.00	2.00	2.00	2.00	2.00	2.00	2.00
Na	0.11	0.35	0.26	0.34	0.46	0.45	0.51	0.46
K	0.06	0.05	0.06	0.05	0.05	0.06	0.03	0.06
ΣA	0.17	0.40	0.33	0.38	0.50	0.51	0.54	0.51
Species	*Tsch*	*Tsch*	*Tsch*	*Tsch*	*Prg*	*Prg*	*Prg*	*Prg*

No.	9	10	11	12	13	14	15
Sample	D05-6	D05	D05	D12	D12	D13	D13
SiO_2	51.86	50.10	51.99	48.05	45.61	46.12	49.49
TiO_2	0.22	0.14	0.23	0.33	0.27	0.23	0.25
Al_2O_3	6.31	8.67	5.47	9.79	13.39	13.04	9.36
MnO	0.37	0.22	0.31	0.19	0.22	0.16	0.14
FeO*	13.24	11.18	13.67	15.09	15.44	13.92	13.04
Fe_2O_3*	0.24	1.40	0.59	2.16	1.93	2.60	1.33
MgO	13.89	13.68	13.50	10.18	8.60	9.76	12.42
CaO	11.50	12.05	11.79	11.30	11.32	11.11	11.22
Na_2O	0.25	0.40	0.33	0.81	1.04	0.87	0.60
K_2O	0.10	0.12	0.08	0.10	0.20	0.18	0.12
H_2O**	2.05	2.04	2.04	2.00	2.00	2.01	2.04
Total	100.00	100.00	100.00	100.00	100.00	100.00	100.00
Cation numbers based on 23 oxygens							
Si	7.45	7.17	7.50	7.03	6.70	6.72	7.13
Al	0.55	0.83	0.50	0.97	1.30	1.28	0.87
ΣT	8.00	8.00	8.00	8.00	8.00	8.00	8.00
Ti	0.02	0.02	0.02	0.04	0.03	0.03	0.03
Al	0.51	0.64	0.43	0.72	1.01	0.96	0.72
Fe^{3+}	0.03	0.15	0.06	0.24	0.21	0.29	0.14
Mn^{2+}	0.00	0.00	0.00	0.00	0.00	0.00	0.00
Fe^{2+}	1.46	1.28	1.58	1.79	1.86	1.60	1.44
Mg	2.97	2.92	2.90	2.22	1.88	2.12	2.67
ΣC	5.00	5.00	5.00	5.00	5.00	5.00	5.00
Mn^{2+}	0.05	0.03	0.04	0.02	0.03	0.02	0.02
Fe^{2+}	0.13	0.06	0.07	0.05	0.03	0.09	0.13
Ca	1.77	1.85	1.82	1.77	1.78	1.74	1.73
Na	0.06	0.06	0.07	0.15	0.16	0.15	0.12
ΣB	2.00	2.00	2.00	2.00	2.00	2.00	2.00
Na	0.01	0.05	0.02	0.08	0.14	0.09	0.05
K	0.02	0.02	0.01	0.02	0.04	0.03	0.02
ΣA	0.03	0.07	0.04	0.10	0.17	0.13	0.07
Species	*Mg-hb*	*Mg-hb*	*Mg-hb*	*Mg-hb*	*Mg-hb*	*Mg-hb*	*Mg-hb*

No.	16	17	18	19	20	21	22

307
308

Table 4 (*continued*)

Sample	D30	D30	D31-5	D05	D12	D13	D31-6
SiO_2	44.79	52.41	44.09	53.60	55.85	56.02	55.26
TiO_2	0.47	0.17	0.66	0.09	0.05	0.05	0.10
Al_2O_3	14.66	5.90	13.10	2.94	0.83	1.41	2.66
MnO	0.00	0.00	0.21	0.64	0.24	0.18	0.12
FeO*	10.50	5.82	12.27	16.28	12.96	12.09	8.76
Fe_2O_3*	2.75	3.61	2.70	0.00	0.00	0.00	0.49
MgO	12.07	17.74	11.00	12.71	15.86	16.48	18.30
CaO	9.98	10.70	12.36	11.56	11.98	11.61	11.85
Na_2O	2.51	1.42	1.40	0.13	0.15	0.07	0.32
K_2O	0.22	0.16	0.21	0.04	0.03	0.03	0.06
H_2O**	2.03	2.08	2.00	2.02	2.06	2.07	2.08
Total	100.00	100.00	100.00	100.00	100.00	100.00	100.00
Cation numbers based on 23 oxygens							
Si	6.46	7.36	6.46	7.79	7.98	7.96	7.77
Al	1.54	0.64	1.54	0.21	0.02	0.04	0.24
ΣT	8.00	8.00	8.00	8.00	8.00	8.00	8.00
Ti	0.05	0.02	0.07	0.01	0.01	0.01	0.01
Al	0.96	0.33	0.72	0.30	0.12	0.19	0.21
Fe^{3+}	0.30	0.38	0.30	0.00	0.00	0.00	0.05
Mn^{2+}	0.00	0.00	0.00	0.00	0.00	0.00	0.00
Fe^{2+}	1.10	0.56	1.50	1.94	1.49	1.31	0.90
Mg	2.60	3.71	2.40	2.76	3.38	3.49	3.83
ΣC	5.00	5.00	5.00	5.00	5.00	5.00	5.00
Mn^{2+}	0.00	0.00	0.03	0.08	0.03	0.02	0.01
Fe^{2+}	0.17	0.13	0.00	0.04	0.06	0.12	0.13
Ca	1.54	1.61	1.94	1.80	1.83	1.77	1.78
Na	0.28	0.26	0.03	0.04	0.04	0.02	0.07
ΣB	2.00	2.00	2.00	1.96	1.96	1.93	2.00
Na	0.42	0.13	0.37	0.00	0.00	0.00	0.02
K	0.04	0.03	0.04	0.01	0.01	0.01	0.01
ΣA	0.46	0.15	0.40	0.01	0.01	0.01	0.03
Species	Mg-hb	Mg-f-hb	Mg-hb	Act	Act	Act	Act

* Total Fe was measured as FeO. FeO/Fe_2O_3 ratio was calculated with ACES_2 Excel spreadsheet (after Locock, 2014).
** H_2O was calculated from the stoichiometry: OH = 2 *apfu*.

Based on the mineral assemblage and textural relationships, two metamorphic events can be recognized in both groups. In *Group1*, the M1 event is featured by the greenschist-amphibolite facies assemblage involving zoned Ca-amphibole with lower Al(tot). The M2 event is represented by higher Al(tot) values, indicating a progressive increase of pressure and temperature from the greenschist-amphibolite boundary to the amphibolite facies. In *Group2* the amphibolite facies M1 event was followed by the M2 event which was a retrograde stage of greenschist metamorphism recorded by the appearance of actinolite rimmed magnesio-hornblende, tschermakite, pargasite or sadanagaite and by the formation of albite, chlorite, epidote and titanite.

4.2. Possible provenance fields

Our petrological and mineralogical data were compared to the amphibolite bodies of Gemericum, Veporicum, Tatricum and Zemplinicum in Slovakia (Fig. 2) (Král' et al.,1997). Since amphibolite is a common and abundant raw material, the largest and the nearest amphibolite bodies are assumed to be the material sources for the investigated amphibolite stone implements. According to Přichystal (2013), stone raw material of polished implements could also have originated from riverbeds, furthermore Török (1996) declares that amphibolite is one of the most common pebble in Slaná- and Hornád-riverbeds; so the major rivers of Slovakia are also plotted on the map (Fig. 2).

The bulk chemistries of Gemericum, Veporicum and Tatricum amphibolites are very similar to each other and also to that of our samples, having subalkaline, tholeiitic character (Fig. 3) (Bajanik & Hovorka, 1981, Hovorka et al., 1993, Ivan et al., 2001, Faryad et al., 2005, Ivan & Méres, 2015). On the

330   AFM diagram, the distribution of the data of the samples and the data of the possible provenance

331   fields overlap each other (Fig. 4) (Bajanik & Hovorka, 1981, Hovorka et al., 1993, Ivan et al., 2001,

332   Faryad et al., 2005, Ivan & Méres, 2015). Using only the major element composition of bulk chemistry,

333   the provenance field cannot be specified. Magnesio-hornblende and actinolite are very common

334   minerals in amphibolites. Based only on their presence, selecting the provenance field is nearly

335   impossible. Regarding the fact that systematic archaeometrical work on amphibolite implements has

336   not been done which we could compare to, we have used various diagnostic minerals as well as the

337   typical thermobarometric P-T data of the amphiboles for comparison to the data of the possible source

338   regions.

339   All the above lithotectonic units where amphibolite occurs show multiphase (Variscan and

340   Alpine) metamorphic evolutions with various intensities. Some localities do not show traces of the

341   Alpine overprint at all, while others did not preserve relict textures of the Variscan metamorphic event

342   (Bezák et al., 1993, Hovorka et al., 1993). Prograde textured amphibolites were preserved in some

343   outcrops in the Ochtiná group (Novotná et al., 2015) and some places in the Veporicum and Tatricum

344   (Krist et al., 1992). Most of the amphibolite occurrences show a retrograde overprint as well. The two

345   subsequent metamorphic events can be characterized by significantly different metamorphic

346   gradients. For the Variscan event 40 °C/km is typical, while the Alpine event suggests 10 °C/km (Bezák

347   et al., 1993). The results of the thermobarometric calculations (according to Gerya et al., 1997, Zenk

348   and Schulz 2004) (Fig. 12) show that all the studied samples fit well to the Variscan metamorphic

349   gradient (Bezák et al., 1993); no trace of a high pressure, low-medium temperature overprint is

350   observable. The Variscan metamorphic gradient (Bezák et al., 1993) (Fig. 12) and the Variscan P-T loop

351   (Putiš et al., 1997) (Fig. 13) cover all the available fields that are considered here as possible source

352   regions for the present group of amphibolite polished implements. The thermobarometric data of

353   some possible provenance fields and the samples fit each other well as shown in Fig. 13. Regarding

354   Tatricum, the Little Carpathians can be considered as a possible source region, while the

355   thermobarometric data of Tribeč Mountains exclude these fields as source regions (Fig. 13).

Table 5
Chemical composition of amphiboles (*Group 2*).

No.	1	2	3	4	5	6	7	8	9	10
Sample	B12-20	B12-26	B12-31	B12-20	B12-16	B12-17	D17-18	D47-21	D47-22	D47-23
SiO_2	40.72	40.73	40.35	40.72	41.49	42.34	42.46	39.99	39.48	39.90
TiO_2	0.06	0.45	0.00	0.06	0.16	0.05	0.06	0.60	0.44	0.44
Al_2O_3	19.68	19.07	19.86	19.68	18.06	17.14	15.56	17.52	18.23	18.68
MnO	0.00	0.00	0.05	0.00	0.06	0.00	0.26	0.39	0.45	0.42
FeO*	15.01	14.10	14.00	15.01	14.09	14.33	15.92	16.30	16.72	16.17
Fe_2O_3*	1.55	1.66	1.69	1.55	1.70	1.52	1.44	0.96	1.25	0.74
MgO	7.48	8.35	8.21	7.48	8.77	8.96	8.47	7.75	7.20	7.16
CaO	11.12	10.90	11.00	11.12	11.15	10.92	11.20	10.15	9.99	9.92
Na_2O	2.29	2.60	2.68	2.29	2.30	2.59	2.30	3.31	3.20	3.48
K_2O	0.11	0.15	0.17	0.11	0.23	0.15	0.35	1.07	1.08	1.10
H_2O**	1.99	2.00	2.00	1.99	2.00	2.00	1.98	1.96	1.95	1.97
Total	100.00	100.00	100.00	100.00	100.00	100.00	100.00	100.00	100.00	100.00
Cation numbers based on 23 oxygens										
Si	6.01	6.00	5.94	6.01	6.11	6.23	6.31	6.03	5.98	6.00
Al	2.00	2.01	2.06	2.00	1.89	1.78	1.69	1.97	2.02	2.00
ΣT	**8.00**	**8.00**	**8.00**	**8.00**	**8.00**	**8.00**	**8.00**	**8.00**	**8.00**	**8.00**
Ti	0.01	0.05	0.00	0.01	0.02	0.01	0.01	0.07	0.05	0.05
Al	1.42	1.30	1.39	1.42	1.24	1.20	1.04	1.15	1.23	1.31
Fe^{3+}	0.17	0.18	0.19	0.17	0.19	0.17	0.16	0.11	0.14	0.08
Mn^{2+}	0.00	0.00	0.00	0.00	0.00	0.00	0.00	0.00	0.00	0.01
Fe^{2+}	1.75	1.63	1.62	1.75	1.63	1.67	1.92	1.93	1.95	1.95
Mg	1.65	1.83	1.80	1.65	1.92	1.97	1.88	1.74	1.63	1.61
ΣC	**5.00**	**5.00**	**5.00**	**5.00**	**5.00**	**5.00**	**5.00**	**5.00**	**5.00**	**5.00**
Mn^{2+}	0.00	0.00	0.01	0.00	0.01	0.00	0.03	0.05	0.06	0.05
Fe^{2+}	0.10	0.11	0.10	0.10	0.10	0.10	0.06	0.01	0.02	0.00
Ca	1.76	1.72	1.74	1.76	1.76	1.72	1.78	1.64	1.62	1.60
Na	0.14	0.18	0.16	0.14	0.13	0.18	0.13	0.30	0.30	0.36
ΣB	**2.00**	**2.00**	**2.00**	**2.00**	**2.00**	**2.00**	**2.00**	**2.00**	**2.00**	**2.00**
Na	0.51	0.57	0.61	0.51	0.52	0.56	0.54	0.67	0.64	0.66
K	0.02	0.03	0.03	0.02	0.04	0.03	0.07	0.21	0.21	0.21
ΣA	0.53	0.60	0.64	0.53	0.57	0.58	0.60	0.88	0.85	0.87
Species	*F-sdg*	*Sdg*	*Sdg*	*F-sdg*	*Prg*	*Prg*	*Fprg*	*Fprg*	*Fprg*	*Fprg*

No.	11	12	13	14	15	16	17	18	19	20
Sample	D08-5	C02-25	B05-42	D08-29	D15-4	D17-44	C02-11	B05-27	D08-30	D15-2
SiO_2	40.24	49.72	49.65	47.48	47.19	52.80	50.94	52.89	53.51	52.82
TiO_2	0.00	0.00	0.13	0.08	0.03	0.08	0.03	0.07	0.11	0.00
Al_2O_3	14.28	5.99	8.83	10.88	12.12	5.07	4.87	4.12	4.66	5.06
MnO	0.20	0.14	0.00	0.28	0.09	0.32	0.26	0.00	0.27	0.16
FeO*	18.48	22.82	12.01	10.46	12.51	14.10	20.58	17.83	8.99	9.53
Fe_2O_3*	10.07	0.03	2.50	3.82	1.19	1.00	0.12	0.00	1.09	1.42
MgO	6.73	7.45	12.81	12.65	11.47	13.18	9.23	11.78	17.05	16.03
CaO	7.52	11.64	11.03	11.34	11.64	10.14	11.65	10.83	11.79	12.34
Na_2O	0.25	0.13	0.97	0.85	1.27	1.11	0.21	0.48	0.41	0.54
K_2O	0.23	0.14	0.04	0.15	0.47	0.17	0.12	0.00	0.06	0.05
H_2O**	1.91	1.95	2.03	2.03	2.03	2.04	1.98	2.01	2.07	2.06
Total	99.91	100.00	100.00	100.00	100.00	100.00	100.00	100.00	100.00	100.00
Cation numbers based on 23 oxygens										
Si	6.12	7.47	7.14	6.85	6.83	7.61	7.58	7.71	7.56	7.50
Al	1.88	0.53	0.86	1.15	1.17	0.39	0.42	0.29	0.44	0.50
ΣT	**8.00**	**8.00**	**8.00**	**8.00**	**8.00**	**8.00**	**8.00**	**8.00**	**8.00**	**8.00**
Ti	0.00	0.00	0.01	0.01	0.00	0.01	0.00	0.01	0.01	0.00
Al	0.68	0.53	0.64	0.69	0.90	0.47	0.43	0.42	0.33	0.35
Fe^{3+}	1.15	0.00	0.27	0.41	0.13	0.11	0.01	0.00	0.12	0.15
Mn^{2+}	0.00	0.00	0.00	0.00	0.00	0.00	0.00	0.00	0.00	0.00
Fe^{2+}	1.64	2.79	1.33	1.17	1.49	1.58	2.51	2.01	0.95	1.11
Mg	1.53	1.67	2.75	2.72	2.48	2.83	2.05	2.56	3.59	3.39
ΣC	**5.00**	**5.00**	**5.00**	**5.00**	**5.00**	**5.00**	**5.00**	**5.00**	**5.00**	**5.00**
Mn^{2+}	0.03	0.02	0.00	0.04	0.01	0.04	0.03	0.00	0.03	0.02
Fe^{2+}	0.71	0.07	0.12	0.10	0.03	0.12	0.05	0.17	0.11	0.02
Ca	1.23	1.87	1.70	1.75	1.81	1.57	1.86	1.69	1.78	1.88
Na	0.04	0.04	0.18	0.12	0.16	0.27	0.06	0.14	0.08	0.08
ΣB	**2.00**	**2.00**	**2.00**	**2.00**	**2.00**	**2.00**	**2.00**	**1.99**	**2.00**	**2.00**
Na	0.04	0.00	0.09	0.12	0.20	0.04	0.00	0.00	0.04	0.07
K	0.05	0.03	0.01	0.03	0.09	0.03	0.02	0.00	0.01	0.01
ΣA	0.08	0.03	0.10	0.15	0.29	0.07	0.03	0.00	0.05	0.08
Species	*F-f-tsch*	*Fhb*	*Mg-hb*	*Mg-hb*	*Mg-hb*	*Mg-hb*	*Fact*	*Act*	*Act*	*Act*

* Total Fe was measured as FeO. FeO/Fe_2O_3 ratio was calculated with ACES_2 Excel spreadsheet (after Locock, 2014).
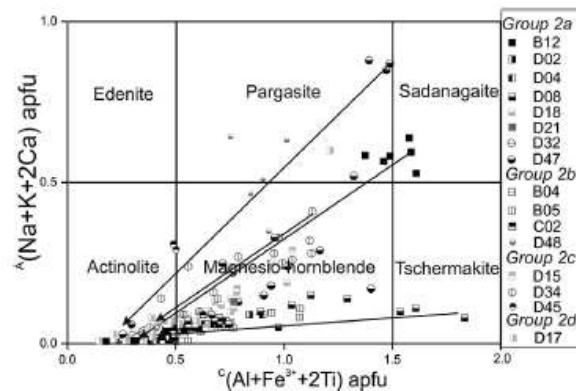** H_2O was calculated from the stoichiometry: OH = 2 *apfu*.

356
357

Fig. 9. Chemical composition of calcic amphiboles of *Group2* and their potential provenances plotted in the ^{C}(Al + Fe^{3+} +2Ti) vs ^{A}(Na + K + 2Ca) diagram. The arrows indicate the phase changes from core to rim. Circles signify the samples analysed by the "surface method".
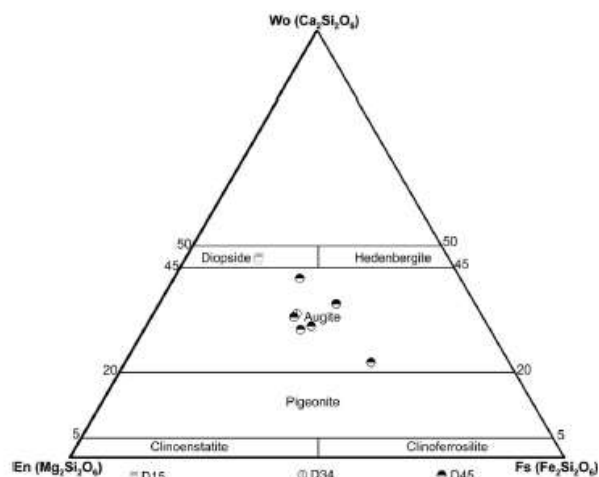
358
359

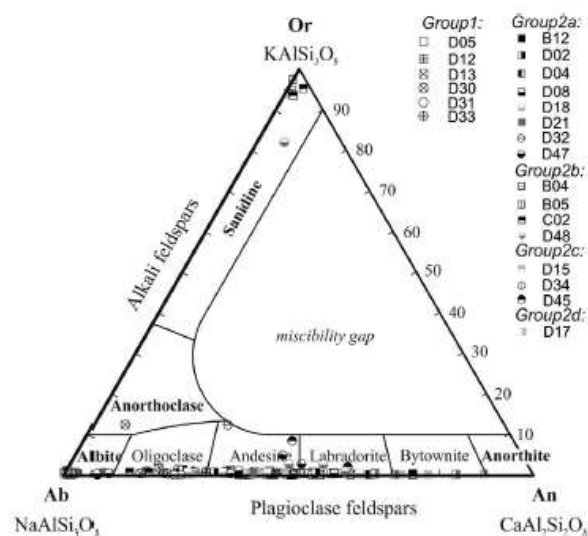**Fig. 10.** Clinopyroxene compositions of D15, D34, D45 samples plotted in the En-Fs-Wo ternary diagram (Morimoto, 1989).

360
361

Fig. 11. Compositions of feldspars plotted in Or-Ab-An ternary diagram.

362
363

364   In *Group1* the tschermakite- and pargasite-bearing prograde textured samples reached the

365   highest metamorphic grade. In *Group1* the estimated thermobarometric data mostly range 540-635

366   °C and 5-6.2 kbar. But the D33 sample has a lower T_{max} 460 °C and $P_{(Tmax)}$ 2.8 kbar. Comparing to the

367   prograde textured amphibolites from the Ochtiná group (Novotná et al., 2015) and sporadically from

368   Veporicum and Tatricum (Krist et al., 1992) the majority of these *Group1* samples very likely originated

369   from one of these areas (Table 10). According to the P-T estimation of D30 and D31, they correlate

370   obviously to GAC-Klátov. D05, D12, D13 samples fit well to the Ochtiná group, but the P-T data of the

371   Branisko, Čierna Hora, Čierny Balog, Little Carpathians and GAC-Klátov territories also match well. The

372   D33 implement can be originated not only from Ochtiná group but Čierna Hora too (Fig. 13) (Table 10).

373   In the B12 sample (*Group2a*), besides the ordinary amphiboles, the uncommon sadanagaite

374   and ferro-sadanagaite, as well as pargasite and ferro-pargasite also appear. The compositional range

375   of these rare amhiboles is equivalent to pargasite and tschermakite, respectively, according to the

376   previous nomenclature of amphiboles (Leake et al., 1997). Tschermakite, pargasite and their ferroan

377   counterparts were found in several samples: D05, D30, D31 (*Group1*), B12, D08, D47 (*Group2a*), D45

378   (*Group2c*), D48 (*Group2b*), D17 (*Group2d*). These samples have reached the highest metamorphic

379   temperature (Fig. 12, Table 9). Results on pargasite-bearing Variscan amphibolites were published by

380   Radvanec et al. (2017) in the GAC (Gneiss-Amphibolite Complex), Klátov area. Tschermakite-bearing

381   amphibolites occur in several localities: the Ochtiná group (Novotná et al., 2015), Čierny Balog (Putiš

382   et al. 1997), Čierna Hora (Faryad & Jacko, 2002) and also the Little Carpathians (Ivan et al., 2001). The

383   calculated thermobarometric data of B12 and D47 samples would agree with the material originated

384   from Zemplinicum or GAC-Klátov regions. The estimated P-T data and the mineral assemblage of D17

385   and D48 pargasite-bearing implements fit well to GAC-Klátov, but the Ochtiná group, Branisko

386   Mountains and even the distant Little Carpathians cannot be excluded. The D08 (*Group2*) sample

387   matches well to the Ochtiná group, Branisko or the Little Carpathians, but Stražovské Mountains can

388   be considered also (Fig. 13) (Table 10).

389   Two epidote-rich amphibolite implements, D02 and D04 samples (*Group2a*) can be originated

390   from Ochtiná group or GAC-Klátov. The calculated T_{max} ≈500 °C and $P_{(Tmax)}$ ≈3.7 kbar are similar for the

391   two stone implements (Fig. 13).

392   The D18, D21 and D32 samples from *Group2a*, have a very common amphibolite mineral

393   assemblage without any diagnostic minerals and their estimated P-T data overlap with earlier

394   published thermobarometric data of numerous possible provenance fields: Branisko Mountains,

395   Čierna Hora, Octhiná group, GAC-Klátov or even with the Little Carpathians. (Fig. 13).

396   Potassic feldspar is present as a relict phase in *Group2b*. Hence this variety may be correlated

397   to Čierna Hora and Branisko Mountains (Faryad & Jacko, 2002) amphibolites as these rocks contain

398   potassic feldspar and Mn-bearing ilmenite as accessory phases. Furthermore, plagioclase with a

399   maximum An_{43} content was mentioned from here. The C02 sample contains bytownite as a relict phase

400   also. The plagioclase compositions of these three stone tools and their mineral assemblages are rather

401   similar to the amphibolites of Čierna Hora. Amphibolites from Čierna Hora have a tholeiitic basalt and

402   basaltic andesite composition (Faryad et al., 2005), similar to the above mentioned three implements.

403   The well-matching thermobarometry data of *Group2b* and Čierna Hora confirm the correlation (Figs.

404   6—G, E, 14). In the case of the D48 sample the estimated P-T values indicate Branisko Mountain as a

405   possible provenance field, but the Ochtiná group and GAC-Klátov cannot be excluded either (Table 10).

406   *Group2c* corresponds to clinopyroxene- and biotite-bearing amphibolites described from

407   Gemericum (Faryad, 1997, Hovorka & Spišiak, 1997). The mineral assemblage and the estimated

408   thermobarometry data of *Group2c* indicate GAC-Klátov as a possible provenance field, but Branisko

409   Mountain, Čierna Hora and Little Carpathians cannot be excluded because of the matching P-T data.

410   Biotite-bearing amphibolites were earlier investigated from the above-mentioned territories

411   (Vozárová & Faryad, 1997, Ivan et al., 2001) (Fig. 13).

412   Higher magnetic susceptibility values were measured from some samples of *Group1* (D33) and

413   *Group2* (B12, C02, D04, D08, D18), although the presence of magnetite was not always supported by

414   the EDS/SEM observations. Greenstones and amphibolites with high magnetite content were

415   described from the Little Carpathians (Ivan et al., 2001) and the Slovak Ore Mountains (Faryad &

416   Peterec, 1987). Therefore, the raw material of these polished stone tools might originate from these

417   territories (Table 10).

418   The schematic map of amphibolite outcrops and the major rivers shows that the Hornád- and

419   Slaná rivers cross the Gemericum, Veporicum and Zemplinicum regions and flow to Borsod-Abaúj-

420   Zemplén county, the archaeological collecting territory of the investigated amphibolite implements

421   (Fig. 2). This confirms these rivers as deliverers of raw materials from the source areas.

Table 6
Chemical composition of epidotes.

No.	1	2	3	4	5	6	7	8	9	10
Sample	B12	D02	D02	D04	D04	D08	D08	D15	D15	D17
SiO_2	39.52	39.36	39.32	39.13	39.15	38.44	38.83	38.66	39.26	38.83
TiO_2	0.00	0.07	0.46	0.04	0.00	0.00	0.03	0.04	0.08	0.16
Al_2O_3	25.43	26.82	28.95	27.05	29.63	23.82	29.75	27.69	29.52	23.69
$Fe_2O_3^*$	11.04	10.10	7.22	9.52	6.54	13.53	6.72	8.81	6.40	13.24
MnO	0.00	0.00	0.09	0.07	0.00	0.10	0.00	0.06	0.08	0.12
MgO	0.37	0.09	0.07	0.27	0.30	0.17	0.26	0.28	0.41	0.04
CaO	21.46	21.54	21.86	21.79	22.25	21.92	22.37	22.43	21.99	21.95
Na_2O	0.18	0.00	0.00	0.14	0.14	0.06	0.05	0.05	0.25	0.00
K_2O	0.07	0.10	0.09	0.06	0.05	0.06	0.06	0.06	0.07	0.07
H_2O^{**}	1.92	1.92	1.94	1.92	1.94	1.90	1.93	1.92	1.94	1.90
Total	100.00	100.00	100.00	100.00	100.00	100.00	100.00	100.00	100.00	100.00
Cation numbers based on 12.5 oxygens										
Si	3.08	3.06	3.03	3.01	3.01	3.04	2.99	3.00	3.02	3.06
ΣT	3.08	3.06	3.03	3.01	3.01	3.04	2.99	3.00	3.02	3.06
Ti	0.00	0.00	0.03	0.00	0.00	0.00	0.00	0.00	0.00	0.01
Al	2.34	2.46	2.63	2.45	2.69	2.22	2.69	2.54	2.68	2.20
Fe^{3+}	0.65	0.59	0.42	0.55	0.38	0.80	0.39	0.52	0.37	0.79
Mg	0.00	0.00	0.00	0.00	0.00	0.00	0.00	0.00	0.00	0.00
ΣM	2.99	3.05	3.08	3.00	3.07	3.02	3.08	3.06	3.05	3.00
Mn^{2+}	0.00	0.00	0.01	0.00	0.00	0.01	0.00	0.00	0.01	0.01
Mg	0.04	0.01	0.01	0.03	0.03	0.02	0.03	0.03	0.05	0.00
Ca	1.79	1.79	1.80	1.80	1.83	1.86	1.85	1.87	1.81	1.86
Na	0.03	0.00	0.00	0.02	0.02	0.01	0.01	0.01	0.04	0.00
K	0.01	0.01	0.01	0.01	0.00	0.01	0.01	0.01	0.01	0.01
ΣA	1.87	1.81	1.83	1.86	1.88	1.91	1.90	1.92	1.92	1.88
Species	Ep	Ep	Czo	Ep	Czo	Ep	Czo	Ep	Czo	Ep

* Total Fe was measured as Fe_2O_3.
** H_2O was calculated from the stoichiometry: OH = 1 *apfu*.

Table 7
Chemical composition of biotites.

No.	1	2	3	4
Sample	D15	D17	D17	D17
SiO_2	39.72	38.09	39.79	39.06
TiO_2	0.17	0.22	0.15	0.15
Al_2O_3	16.42	18.55	16.70	17.45
FeO^*	14.49	14.18	13.20	13.33
MnO	0.06	0.12	0.12	0.10
MgO	15.59	15.19	16.24	16.38
CaO	0.50	0.11	0.15	0.17
Na_2O	0.20	0.06	0.00	0.00
K_2O	8.75	9.39	9.52	9.25
H_2O^{**}	4.10	4.10	4.11	4.11
Total	100.00	100.00	100.00	100.00
Cation numbers based on 11 oxygens				
Si	2.90	2.79	2.90	2.85
Al	1.10	1.21	1.10	1.15
ΣT	4.00	4.00	4.00	4.00
Al	0.32	0.39	0.33	0.35
Ti	0.01	0.01	0.01	0.01
Fe^{2+}	0.89	0.87	0.81	0.81
Mn	0.00	0.01	0.01	0.01
Mg	1.70	1.66	1.77	1.78
ΣM	2.92	2.95	2.93	2.96
Ca	0.04	0.01	0.01	0.01
Na	0.03	0.01	0.00	0.00
K	0.82	0.88	0.89	0.86
ΣI	0.88	0.90	0.90	0.87

* Total Fe was measured as FeO.
** H_2O was calculated from the stoichiometry: OH = 2 *apfu*.

Conclusions

Based on the mineralogical assemblages and textural relations of the amphibolite stone implements, two groups have been distinguished: *Group1* and *Group2*. Six samples preserving the features of prograde metamorphism were assigned to *Group1*. *Group2* contains most of the samples which are overprinted by retrograde metamorphism. The results of thermobarometric calculations of the investigated polished stone tools were compared to the earlier published thermobarometric data for

432 the amphibolite field samples, as expressed in the Variscan metamorphic gradient (Fig. 12) and in

433 Variscan P-T loop (Fig. 13).

Table 8
Chemical composition of chlorites.

No.	1	2	3	4	5	6	7	8	9	10
Sample	D13	D13	C02	C02	D04	D02	D02	D21	D21	D21
SiO_2	27.77	30.38	29.69	29.63	27.12	27.84	29.99	20.88	20.33	24.52
TiO_2	0.13	0.07	0.04	0.09	0.02	0.04	0.00	0.00	0.00	0.00
Al_2O_3	21.63	20.36	18.72	18.98	20.66	19.91	20.22	13.31	16.19	15.24
Fe_2O_3*	0.00	0.00	0.00	0.00	0.00	0.00	0.00	13.29	13.07	4.90
FeO*	20.68	19.87	26.95	26.37	37.45	29.04	28.14	39.53	34.52	39.39
MnO	0.08	0.13	0.35	0.30	0.12	0.20	0.08	0.08	0.00	0.00
MgO	17.65	15.41	11.52	12.21	3.44	11.57	10.03	2.55	5.27	4.74
CaO	0.20	1.64	1.20	0.79	0.25	0.00	0.00	0.13	0.05	0.25
Na_2O	0.03	0.22	0.00	0.00	0.00	0.00	0.00	0.13	0.19	0.32
K_2O	0.02	0.04	0.07	0.12	0.00	0.03	0.03	0.04	0.02	0.19
H_2O**	11.82	11.87	11.47	11.51	10.93	11.37	11.51	10.07	10.36	10.46
Total	100.00	100.00	100.00	100.00	100.00	100.00	100.00	100.00	100.00	100.00
Cation numbers based on 14 oxygens										
Si	2.82	3.07	3.11	3.09	2.98	2.94	3.13	2.49	2.35	2.81
Al	1.18	0.93	0.89	0.91	1.02	1.06	0.87	1.51	1.65	1.19
ΣT	4.00	4.00	4.00	4.00	4.00	4.00	4.00	4.00	4.00	4.00
Al	1.41	1.49	1.41	1.42	1.65	1.41	1.61	0.36	0.56	0.87
Ti	0.01	0.01	0.00	0.01	0.00	0.00	0.00	0.00	0.00	0.00
Fe^{3+}	0.00	0.00	0.00	0.00	0.00	0.00	0.00	1.19	1.14	0.42
Fe^{2+}	1.76	1.68	2.36	2.30	3.44	2.56	2.45	3.93	3.34	3.77
Mn	0.01	0.01	0.03	0.03	0.01	0.02	0.01	0.01	0.00	0.00
Mg	2.67	2.32	1.80	1.90	0.56	1.82	1.56	0.45	0.91	0.81
Ca	0.02	0.18	0.13	0.09	0.03	0.00	0.00	0.02	0.01	0.03
Na	0.01	0.04	0.00	0.00	0.00	0.00	0.00	0.03	0.04	0.07
K	0.00	0.01	0.01	0.02	0.00	0.00	0.00	0.01	0.00	0.03
ΣM	5.88	5.74	5.74	5.75	5.69	5.82	5.63	6.00	6.00	6.00

* Total Fe was measured as FeO. FeO/Fe_2O_3 ratio was calculated from the stoichiometry: ΣM = 6.00 *apfu*.
** H_2O was calculated from the stoichiometry: OH = 8 *apfu*.

434

435

436

437

438 Metamorphic evolution, thermobarometric data, petrographic-, and mineralogical observations have

439 been taken into account in the classification of the possible provenance fields of the amphibolite

440 polished stone implements. Even the distance of the source area and the archaeological localities is

441 not a negligible factor because amphibolite is a diverse, common and a widespread rock in Slovakia.

442 According to this fact, we suppose that the nearby amphibolite outcrops may be considered

443 particularly (Table 10) For the *Group1* and for the D02, D04 samples of *Group2a* Ochtina group and

444 GAC Klátov is the most likely provenance fields, but for the *Group1* Veporicum and Tatricum cannot be

445 excluded either. In the case of D04 Little Carpathians is a presumptive area. The B12 and D47 samples

446 (*Group2a*) have reached the highest metamorphic grade, they may originate from GAC-Klátov or the

447 Zemplinicum unit. D08, D18, D21 and D32 samples of *Group2a* may have derived from several fields

448 of Gemericum, Veporicum, Tatricum. The most possibble source areas of the Group2b are Čierna Hora

449 and Branisko, but in the case of C02 sample Tatricum cannot be excluded either, furthermore the D48

450 implement can be originated from GAC-Klátov or Ochtina group too. The samples of Group2c and

451 Group2d most likely stem from GAC Klátov, but the possible provenance field of Group2c may be

452 Branisko, Čierna Hora or the LIttle Carpathians as well (Table 10).

453   To identify the provenance field at site level in the case of amphibolite archaeological findings, cannot

454   be solved without specific minerals or signs except for individual cases. However, because of the

455   overlap of the P-T values of the provenance fields and the uncertainty of the estimated P-T values for

456   the archaeological samples, it is not possible to unambiguously assign any provenance field to any

457   single sample. Based on the mineral assemblages, textural features and thermobarometry estimations

458   it can be concluded that the provenance fields of our samples could be the Gemericum, Veporicum,

459   Tatricum and the Zemplinicum (Figs. 13, 14) (Table 10).

460

Table 9
Thermobarometry data of polished stone tools. MT: Medium-temperature amphibolites; HT: High-temperature amphibolites. *: measured with "original-surface" method.

| Sample	Number of measurements	T_{avg} (°C)	P_{avg} (kbar)	Standard deviation T (°C)	Standard deviation P (kbar)	T_{max} (°C)	$P_{(Tmax)}$ (kbar)
MT							
B04	2	441	2.7	8.49	0.12	450	2.8
B05	3	510	3.9	7.58	0.17	516	4.0
C02	4	442	2.7	12.88	0.18	450	2.8
D02	2	480	3.4	22.45	0.41	500	3.7
D04	1	510	3.7	0.00	0.00	510	3.7
D05	1	540	5.3	0.00	0.00	540	5.3
D09	3	480	3.0	28.36	0.38	510	3.5
D18	3	530	4.0	14.32	0.18	545	4.1
D21	8	540	2.8	18.66	0.18	600	3.4
D32*	1	548	4.0	0.00	0.00	548	4.0
D33*	3	455	2.7	9.73	0.21	460	2.8
HT							
B12	6	670	7.1	12.53	0.30	680	7.3
D08	6	580	4.7	38.66	0.55	600	4.8
D12	3	540	4.7	25.75	0.59	570	5.0
D13	5	520	4.0	28.14	0.56	560	5.0
D15	1	555	4.8	0.00	0.00	555	4.8
D17	1	610	5.7	0.00	0.00	610	5.7
D31*	13	620	5.7	12.94	0.35	635	6.2
D30*	16	588	5.1	21.55	0.48	612	5.6
D34*	6	550	4.5	20.71	0.37	580	5.1
D47*	6	630	6.0	61.46	1.18	690	7.0
D48*	5	580	4.7	7.73	0.08	590	4.60
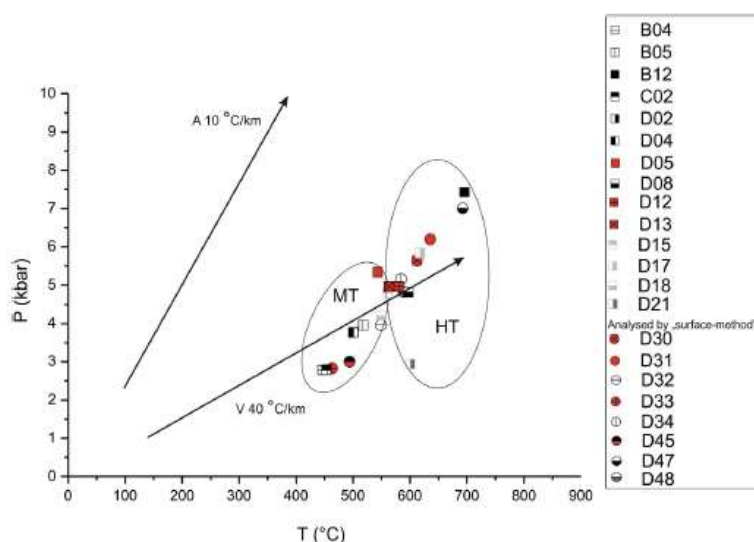
461

462

Fig. 12. P-T diagram showing thermobarometric estimated calculation results T_{max} and $P_{(Tmax)}$ of the amphibolite polished stone tools plotted with the Variscan (V) and Alpine (A) metamorphic gradient (Bezák et al., 1993). Red coloured symbols signify the *Group1* samples, while the other samples are in *Group2*.
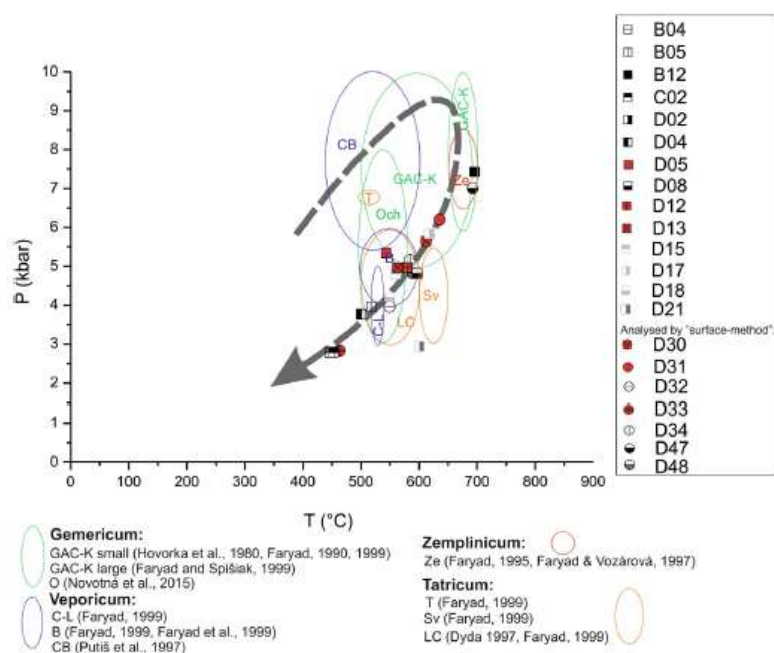
463

464

Fig. 13. Thermobarometric data of amphibolite implements and of field samples from Gemericum, Veporicum, Tatricum and Zemplinicum. The grey loop indicates the estimated Variscan P-T loop (Putiš et al., 1997). Red coloured symbols signify the *Group1* samples, while the other samples are all in *Group2*. Abbreviations: GAC-K: Gneiss Amphibolite Complex, Klátov; C-L: Čierna Hora, lower unit; B: Branisko Mountains; CB: Čieny Balog; Ze: Zemplinicum; T: Tribeč Mountains; Sv: Stražovské Mountains; LC: Little Carpathians. (See above-mentioned references for further information.)

465

466 As amphibolite is a widespread and common rock in Slovakia no correlation has been detected

467 between lithotypes and the typology of the artefacts, furthermore nor in their chronological and

468 cultural aspects.

Table 10

Amphibolite stone implements and their possible provenance fields. (Abbreviations: G1: *Group1*, G2a: *Group2a*, G2b: *Group2b*, G2c: *Group2c*, G2d: *Group2d*). *** the most likely, ** likely, * possible.

Possible provenance fields/Samples	D05-G1	D12-G1	D13-G1	D30-G1	D31-G1	D33-G1	B12-G2a	D02-G2a	D04-G2a	D08-G2a	D18-G2a
Gemericum											
Klátov				***	***		**	**	**	*	*
Gemericum-Veporicum											
Ochtiná group	***	***	***	**	**	**		**	**	*	*
Veporicum	*	*	*	*	*	*					
Branisko										*	*
Čierna Hora						**					*
Čierny Balog											
Tatricum	*	*	*	*	*	*					
Little Carpathians									*	*	*
Tribeč											
Stražovské Mountains										*	
Zemplinicum							**				

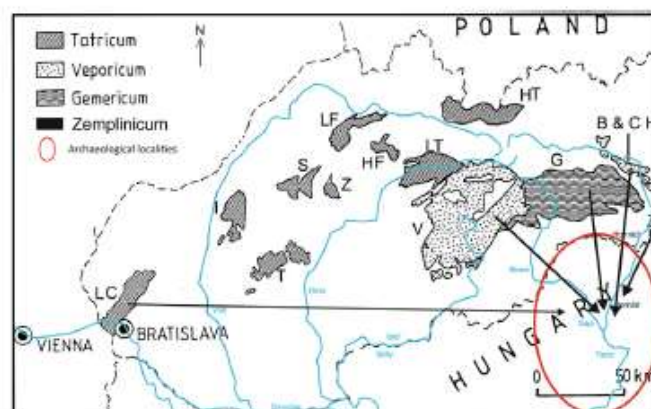| Possible provenance fields/Samples	D21-G2a	D32-G2a	D47-G2a	B04-G2b	B05-G2b	C02-G2b	D48-G2b	D15-G2c	D34-G2c	D45-G2c	D17-G2d
Gemericum											
Klátov	*	*	**				*	***	***	***	**
Gemericum-Veporicum											
Ochtiná group	*	*					*				
Veporicum											
Branisko	*	*		**	**	**	**	*	*	*	
Čierna Hora	*	*		***	***	***		*	*	*	
Čierny Balog											
Tatricum											
Little Carpathians	*	*				*		*	*	*	
Tribeč											
Stražovské Mountains											
Zemplinicum			**								

469

Fig. 14. The schematic geological setting of the amphibolites from the surrounding area after Král' et al., (1997). The arrows show the relation between the possible provenance fields and archaeological localities of the studied stone implements. For the abbreviations on the map, see those on Fig. 13.

References

Bajaník S., Hovorka D. 1981: The amphibolite facies metabasites of the Rakovec group of Gemericum (The Western Carpathians). Geologica Carpathica 32, 679-705.

Bendő Zs., Oláh I., Péterdi B., Szakmány Gy., Horváth E. 2013: Non-destructive SEM-EDX analytical method for polished stone tools and gems: opportunities and limitations. Archeometriai Műhely 10/1, 51-66.

Bezák V., Sassi F. P., Spišiak J, Vozárová A. 1993: An outline of the metamorphic events recorded in the Western Carpathians (Slovakia). Geologica Carpathica 44, 351-364.

Bradák B., Szakmány Gy., Józsa S., Přichystal A. 2009: Application of magnetic susceptibility on polished stone tools from Western Hungary and the Eastern part of Czech Republic (Central Europe). Journal of Archaeological Science 36, 2437-2444. http://dx.doi.org/10.1016/j.jas.2009.07.001.

Csengeri P. 2011: Middle Neolithic face vessels from Garadna (Hornád valley). Herman Ottó Múzeum Évkönyve 50., 67-104. (in Hungarian).

Csengeri P. 2013: Later groups of Alföld Linear Pottery in Northeast of Hungary. (Recent research from Borsod-Abaúj-Zemplén county). Eötvös Lorán University PhD thesis. pp. 311. (in Hungarian).

493 Csengeri P. 2015: Middle Neolithic painted pottery from Borsod-Abaúj-Zemplén county, North-Eastern

494 Hungary, in: Virág C. (Ed.): Neolithic cultural phenomena in the upper Tisza basin international

495 conference, Satu Mare, pp. 127-160.

496 Dyda M. 1997: Disturbance of the Variscan metamorphic complex indicated by mineral reactions, P-T

497 data and crystal size of garnets (Malé Karpaty Mts.), in: Grecula P., Hovorka D., Putiš M. (Eds.),

498 Geological evolution of Western Carpathians., Bratislava, pp. 333-342.

499 Faryad S. W. 1990: Gneiss-amphibolite Complex of the Gemericum. Mineralia Slovaca 22, 303-318.

500 Faryad S. W. 1995: Geothermobarometry of metamorphic rocks from the Zemplinicum (Western

501 Carpathians, Slovakia). Geologica Carpathica 46, 113-123.

502 Faryad S. W. 1997: Metamorphic petrology of the Early Paleozoic low-grade rocks in the Gemericum,

503 in: Grecula P., Hovorka D., Putiš M. (Eds.), Geological evolution of Western Carpathians., Bratislava, pp.

504 309-314.

505 Faryad S. W. 1999: Metamorphic evolution of the eastern part of the Western Carpathians, with

506 emphasis on Meliata Unit. Acta Montanistica Slovaca 4 (2) 148-169.

507 Faryad S. W., Jacko S. 2002: New data on P-T conditions of Variscan and Alpine metamorphism from

508 the Čierna Hora Mts., Veporic Unit, Western Carpathians (Slovakia). Geologica Carpathica 53, Special

509 issue (CD). Proceedings of XVII. Congress of Carpathian-Balkan Geological Association Bratislava,

510 September 1-4, 2002.

511 Faryad S. W., Peterec D. 1987: Manifestations of skarn mineralization in the eastern part of the Spišsko-

512 Gemerské Rudohorie Mts. Geologica Carpathica 38, 111-128.

513 Faryad S. W., Spišiak J. 1999: Klátov-Early Paleozoic amphibolite facies rocks. Acta Montanistica Slovaca

514 4 (2) pp. 173.

515 Faryad S. W., Vozárová A. 1997: Geology and metamorphism of the Zemplinicum basement unit

516 (Western Carpathians), in: Grecula P., Hovorka D., Putiš M. (Eds.), Geological evolution of Western

517 Carpathians., Bratislava, pp. 351-358.

518 Faryad S. W., Vozárová A., Jacko S. 1999: Branisko – amphibolites and gneisses of Tatric and Veporic

519 basement. Acta Montanistica Slovaca 4, 182.

520 Faryad S. W., Ivan P., Jacko S. 2005: Metamorphic petrology of metabasites from the Branisko and

521 Čierna Hora Mountains (Western Carpathians, Slovakia). Geologica Carpathica 56, 3-16.

522 Gerya T. V., Perchuk L. L., Triboulet C., Audren C., Sez'ko A. I. 1997: Petrology of the Tumanshet Zonal

523 Metamorphic Complex, Eastern Sayan. Petrology 5, 503-532.

524 Hawthorne F. C., Oberti R., Harlow G. E., Maresch W. V., Martin R. F., Schumacher J. C., Welch M. D.

525 2012: IMA report: Nomenclature of the amphibole supergroup. American Mineralogist 97, 2031-2048.

526 Hovorka D., Cheben I. 1997: Raw materials of the Neolithic polished stone artefacts from the site Bajč.

527 Mineralia Slovaca 29, 210-217. http://dx.doi.org/10.2138/am.2012.4276.

528 Hovorka D, Spišiak J. 1997: Medium-grade metamorphics of the Gemeric unit (central Western
529 Carpathians). in: Grecula P., Hovorka D., Putiš M. (Eds.), Geological evolution of Western Carpathians,
530 Bratislava, pp. 315-332.

531 Hovorka D., Méres S., Ivan P. 1993: Pre-Alpine Western Carpathians basement complexes: Lithology
532 and geodynamic setting. Mitt. Österr. Geol. Ges., 86, 33-44.

533 Hovorka D., Illášová L., Pavúk J. 2001: Raw materials of Aeneolithic stone polished artifacts found on
534 type locality of the Lengyel culture: Svodín, Slovakia. Mineralia Slovaca 33, 343-350.

535 Irvine T. N., Baragar W. R. A. 1971: A guide to the chemical classification of the common volcanic rocks.
536 Canadian Journal of Earth Sciences 8, 523-548.

537 Ivan P., Méres S. 2015: Geochemistry of amphibolites and related graphitic gneisses from the Suchý
538 and Malá Magura Mountains (central Western Carpathians) – evidence for relics of the Variscan
539 ophiolite complex. Geologica Carpathica 66, 347-360. https://doi.org/10.1515/geoca-2015-0030.

540 Ivan P., Méres Š., Putiš M. Kohút M. 2001: Early Paleozoic metabasalts and metasedimentary rocks
541 from the Malé Karpaty Mts. (Western Carpathians): Evidence for rift basin and ancient oceanic crust.
542 Geologica Carpathica 52, 67-78.

543 Janák M., Hovorka D., Hurai V., Lupták B., Méres Š., Pitoňák P., Spišiak J. 1997: High-pressure relics in
544 the metabasites of the Western Carpathians pre-alpine basement. in: Grecula P., Hovorka D., Putiš M.
545 (Eds.), Geological evolution of Western Carpathians, Bratislava, pp. 301-38.

546 Kalicz N. & Makkai J. 1977: Die Linienbandkeramik in der Groβen Ungarischen Tiefebene, Akadémiai
547 Kiadó, Budapest, pp. 386.

548 Kasztovszky Zs., T. Biró K., Markó A., Dobosi V. 2008: Cold neutron prompt gamma activation analysis
549 – a non-destructive method for characterization of high silica content chipped stone tools and raw
550 materials. Archaeometry 50, 12-19. http://dx.doi.org/10.1111/j.1475-4754.2007.00348.x.

551 Kereskényi E., Kristály F., T. Biró K., Péterdi B., Bendő Zs., Rózsa P. 2015a: The first results of a new
552 project: archaeometrical investigation of Neolithic polished stone tools of Herman Ottó Museum. *Acta*
553 *Mineralogica-Petrographica Abstract Series* 9, 30.

554 Kereskényi E., Kristály F., Fehér B., Rózsa P. 2015b: The first results of the Neolithic polished stone tools
555 of Herman Ottó Museum. From magma genesis to regional lithosphere-forming processes. 6th
556 Petrological and geochemical Meeting. *University of Szeged, Department of Mineralogy, Geochemistry*
557 *and Petrology,* 71-74. (in Hungarian).

558 Kereskényi E., Szakmány Gy., Fehér B., Kasztovszky Zs., Kristály F., Rózsa P. 2018: New archaeometrical
559 results related to Neolithic blueschist stone tools from Borsod-Abaúj-Zemplén County, Hungary.
560 Journal of Archaeological Science: Reports 17, 581-596.

561   Kráľ J., Hess J. C., Kober B., Lippolt H. J. 1997: $^{207}Pb/^{206}Pb$ and $^{40}Ar/^{39}Ar$ age data from plutonic rocks of

562   the Strážovské vrchy Mts. basement, Western Carpathians, in: Grecula P., Hovorka D., Putiš M. (Eds.),

563   Geological evolution of Western Carpathians, Bratislava, pp. 253-260.

564   Krist E., Korikovskij P. S., Putiš M., Janák M., Faryad S. W. 1992: Geology and petrology of metamorphic

565   rocks of the Western Carpathians crystalline complexes, Comenius University, Bratislava, pp. 7.

566   Leake B. E., Wooley A. R., Arps C. E. S., Birch W. D., Gilbert M. C., Grice J. D., Hawthorne F. C., Kato A.,

567   Kisch H. J., Krivovichec V. G., Linthout K., Laird J., Mandarino J. A., Maresch W. V., Nickel E. H., Rock N.

568   M. S., Schumacher J. C., Smith D. C., Stephenson N. C. N., Ungaretti L., Whittaker E. J. W., Youzhi G.

569   1997: Nomenclature of amphiboles: report of the Subcommittee on Amphiboles of the International

570   Mineralogical Association, Commission on New Minerals and Mineral Names. The Canadian

571   Mineralogist 35, 219-246.

572   Locock, A. 2014: An excel spreadsheet to classify chemical analyses of amphiboles following the IMA

573   2012 recommendations. Computers & sciences 62, 1-11. http://dx.doi.

574   org/10.1016/j.cageo.2013.09.011.

575   Méres S., Hovorka D., Cheben I. 2001: Provenience of polished stone artefacts raw materials from the

576   site Bajč-Medzi kanálmi (Neolithic, Slovakia). Slovak Geological Magazin 7, 369-381.

577   Morimoto N. 1989: Nomenclature of pyroxenes. Canadian Mineralogist 27, 143-156.

578   Novotná N., Jeřábek P., Pitra P., Lexa O., Racek M. 2015: Repeated slip along a major decoupling

579   horizon between crustal-scale nappes of the Central Western Carpathians documented in the Ochtiná

580   tectonic mélange. Tectonophysics 646, 50-64.

581   Plašienka D., Grecula P., Putiš M., Kovač M., Hovorka D. 1997: Evolution and structure of the Western

582   Carpathians: an overview. in: Grecula P., Hovorka D., Putiš M. (Eds.), Geological evolution of Western

583   Carpathians, Bratislava, pp. 1-24.

584   Putiš M., Filová S., Korikovsky S. P., Kotov A. B. 1997: Layered metaigneous complex of the Veporic

585   basement with features of the Variscan and Alpine thrust tectonics (the Western Carpathians), in:

586   Grecula P., Hovorka D., Putiš M. (Eds.), Geological evolution of Western Carpathians, Bratislava, pp.

587   175-196.

588   Přichystal A. 2013: Lithic raw materials in prehistoric times of Eastern Central Europe. Masaryk

589   University, Brno. pp. 200.

590   Radvanec M., Németh Z., Král J., Pramuka S. 2017: Variscan dismembered ophiolite suite fragments of

591   Paleo-Tethys in Gemeric unit, Western Carpathians. Mineralia Slovaca 49, 1-48.

592   Révay Zs. 2009: Determining elemental composition using prompt gamma activation

593   analysis. Analytical Chemistry 81, 6851-6859. http://dx.doi.org/10.1021/ac9011705.

594   Selján É. 2005: The Tiszai cultured Szerencs-Taktaföldvár in the late Neolithicum. Diploma thesis,

595   Eötvös Loránd University, Budapest. (in Hungarian).

596   Szakmány Gy., Kasztovszky Zs. 2004: Prompt Gamma Activation Analysis, a new method in the
597   archaeological study of polished stone tools and their raw materials. European Journal of Mineralogy
598   16, 285-295. http://dx.doi.org/10.1127/0935-1221/2004/0016-0285.
599   Szakmány Gy., Kasztovszky Zs., Szilágyi V., Starnini E., Friedel O., T. Biró K. 2011a: Discrimination of
600   prehistoric polished stone tools from Hungary with non-destructive chemical Prompt Gamma
601   Activation Analyses (PGAA). European Journal of Mineralogy 23, 883-893.
602   http://dx.doi.org/10.1127/0935-1221/2011/0023-2148.
603   Szakmány Gy., Starnini E., Horváth F., Bradák B. 2011b: Investigating trade and exchange patterns in
604   prehistory: Preliminary results of the archaeometric analyses of stone artefacts from Tell Gorzsa
605   (South-East Hungary), in: Turbanti-Memmi, I., (Eds.): Proceedings of the 37th International Symposium
606   on Archaeometry, 12th-16th May 2008, Siena, Italy, *Springer*, Berlin Heidelberg, pp. 311-319.
607   Szentmiklósi L., Belgya T., Révay Zs., Kis Z. 2010: Upgrade of the prompt gamma activation analysis
608   and the neutron-induced prompt gamma spectroscopy facilities at the Budapest Research Reactor.
609   Journal of Radioanalytical and Nuclear Chemistry 286, 501–505. http://dx.doi.org/10.1007/s10967-
610   010-0765-4.
611   Török E. (1996): Hazai kavicsmezők anyagának szilárdsága a halmazjellemzők tükrében. (The strength
612   of the Hungarian gravel fields according to set parameters.) Földtani Közlöny 126/1, pp. 117-129 (in
613   Hungarian).
614   Vozárová A., Faryad S., W. 1997: Petrology of Branisko crystalline rock complex in: Grecula P., Hovorka
615   D., Putiš M. (Eds.), Geological evolution of Western Carpathians, Bratislava, pp. 343-350.
616   Zenk M., Schulz B. 2004: Zoned Ca-amphiboles and related P-T evolution in metabasites from the
617   classical Barrovian metamorphic zones in Scotland. Mineralogical Magazine 68, 769-786.

618
619
620
621   Fig. 1: Schematic map showing archaeological localities of amphibolite stone tools that are deposited
622   at the Herman Ottó Museum. Abbreviation: *BAZ*: Borsod-Abaúj-Zemplén.
623   Fig. 2: Geographical setting of the main lithotectonic units containing amphibolite bodies of the
624   Central-Western Carpathians and depicting the principal rivers of Slovakia. The schematic map is
625   modified after Král' et al. (1997). Abbreviations on the map: B & CH: Branisko and Čierna Hora
626   Mountains, G: Gemericum, V: Veporicum, LT: Low Tatras, HT: High Tatras, LF: Low Fatras, HF: High
627   Fatras, S: Strážovské Mountains, Z: Žiar Mountains, I: Inovec Mountains, T: Tribeč Mountains, LC: Little
628   Carpathians.
629   Fig. 3: Amphibolite implements from the Herman Ottó Museum and their potential provenances
630   plotted in the Total Alkali- Silica (TAS) diagram.

631   Fig. 4: AFM diagram of the investigated amphibolite implements and their possible fields of

632   amphibolite localities plotted in AFM (Irvine and Baragar, 1971) diagram. A = alkali (Na_2O+K_2O), F =

633   FeO (total), M = MgO. IAT = island arc tholeiite, MORB = mid-ocean ridge basalt.

634   Fig. 5: A—B Macroscopic and BSE images of the coarse-grained sample D12 (*Group1a*). C—D

635   Macroscopic and BSE images of the coarse-grained sample D13 (*Group1a*). E—F Macroscopic and BSE

636   images of sample D30 (analysed by original surface) (*Group1b*).

637   Fig. 6: A—B Macroscopic and BSE images of the coarse-grained, ilmenite-rich sample D18 (*Group2a*).

638   C— Ilmenite is partly replaced by titanite with magnetite inclusions in the BSE image of the sample

639   D18. D—E Macroscopic and BSE images of the sample B04 (*Group2b*). F—G Macroscopic and BSE

640   images of the sample B05 (*Group2b*). H—I Macroscopic and BSE images of the sample B12 (*Group2a*).

641   Fig. 7: A—B Macroscopic and BSE images of the foliated, epidote-rich D04 sample (*Group2a*). C—D

642   Macroscopic and BSE images of the well-foliated D08 sample (*Group2a*).

643   Fig. 8: Chemical composition of calcic amphiboles of *Group1* amphibolites plotted in the $^C(Al+Fe^{3+}+2Ti)$

644   vs. $^A(Na+K+2Ca)$ diagram. Arrows indicate the phase changes from core to rim.

645   Fig. 9: Chemical composition of calcic amphiboles of *Group2* and their potential provenances plotted

646   in the $^C(Al+Fe^{3+}+2Ti)$ vs. $^A(Na+K+2Ca)$ diagram. The arrows indicate the phase changes from core to rim.

647   Circles signify the samples analysed by the "surface method".

648   Fig. 10: Clinopyroxene compositions of D15, D34, D45 samples plotted in the En-Fs-Wo ternary diagram

649   (Morimoto, 1989).

650   Fig. 11: Compositions of feldspars plotted in Or-Ab-An ternary diagram

651   Fig. 12: P-T diagram showing thermobarometric estimated calculation results T_{max} and $P(_{Tmax})$ of the

652   amphibolite polished stone tools plotted with the Variscan (V) and Alpine (A) metamorphic gradient

653   (Bezák et al., 1993). Red coloured symbols signify the *Group1* samples, while the other samples are in

654   *Group2.*

655   Fig. 13: Thermobarometric data of amphibolite implements and of field samples from Gemericum,

656   Veporicum, Tatricum and Zemplinicum. The grey loop indicates the estimated Variscan P-T loop (Putiš

657   et al., 1997). Red coloured symbols signify the *Group1* samples, while the other samples are all in

658   *Group2*. Abbreviations: GAC-K: Gneiss Amphibolite Complex, Klátov; C-L: Čierna Hora, lower unit; B:

659   Branisko Mountains; CB: Čieny Balog; Ze: Zemplinicum; T: Tribeč Mountains; Sv: Stražovské Mountains;

660   LC: Little Carpathians.

661   Fig. 14: The schematic geological setting of the amphibolites from the surrounding area after Král' et

662   al., (1997). The arrows show the relation between the possible provenance fields and archaeological

663   localities of the studied stone implements. For the abbreviations on the map, see those on Fig. 13.

664

665